We also analyzed the expression of maturation markers, CD86, CD40, and I-A^b, on WT and TNF-$\alpha^{-/-}$ DCs upon TLR4,2 stimulation. No significant difference was detected in the level of mean fluorescence intensity of these expressions between WT and TNF-$\alpha^{-/-}$ DCs. However, the proportion of CD86 positive cells was increased in TNF-$\alpha^{-/-}$ DCs compared to WT DCs. Thus, TNF-α may play a role in the regulation of CD86 expression on DCs.

MAPKs and PI3K/Akt are involved in activation of various transcription factors that promote the IL-10 synthesis in macrophages/monocytes and DCs upon TLR stimulation [36,39,40]. Recently, we demonstrated that MAPK and PI3K/Akt pathways were responsible for the promotion of IL-10 production by BMDCs upon TLR stimulation [34]. It has been reported that TNF-α also activates MAPK and PI3K signaling pathways via TNFR1 [1,2,5–7,37,38]. To explore the mechanism underlying the TNF-α-mediated regulation of IL-10 production by DCs, we analyzed effect of TNF-α on the activity of MAPKs and PI3K in TNF-$\alpha^{-/-}$ DCs upon TLR stimulation. TNF-α markedly enhanced activities of ERK, p38 MAPK, and Akt in TNF-$\alpha^{-/-}$ DCs upon TLR4,2 stimulation at an early phase (at 7 min). Blocking the activation of ERK, p38 MAPK, or PI3K significantly inhibited IL-10 production by TNF-$\alpha^{-/-}$ DCs upon stimulation with TNF-α plus TLR-L. Thus, TNF-α appears to facilitate the TLR-mediated IL-10 production through the activation of ERK, p38 MAPK, and PI3K/Akt pathways in DCs.

It has been reported that p38 MAPK and Akt are activated via RIP1, while JNK was activated via TRAF2 in TNF-α-mediated cellular responses [6]. Thus, we speculate that RIP1 is crucial for the TNF-α-mediated effect on IL-10 production in TNF-$\alpha^{-/-}$ DCs. On the other hand, Vivarelli et al. showed that RIP1 is also involved in TLR4-mediated activation of PI3K-Akt pathway [41]. Thus, TNF-α- and TLR-mediated signaling pathways appear to share the RIP1. Consequently, we could not clarify whether the decrease in IL-10 production in response to MAPK and PI3K inhibitors (Fig. 4) is due to specific inhibition of the TNF-α-mediated signaling. Nonetheless, we believe that our present findings are important to understand a regulation system of IL-10 in DCs in response to TLR stimulation.

Recently, several studies also showed that MAPK- or PI3K-mediated signal is involved in IL-10 production and autocrine IL-10 negatively regulated IL-12 production upon TLR stimulation in macrophages and DCs [40–43]. On the other hand, we have previously reported that LY294002 (a PI3K specific inhibitor) decreases IL-10 production, but shows no effect on IL-12 p40 production upon TLR-stimulation in BMDCs [34]. At present, decrease in IL-10 production by inhibiting PI3K activity showed no significant effect on IL-12 p40 production by TNF-$\alpha^{-/-}$ DCs stimulated with TLR-L plus TNF-α (Fig. 4). The discrepancy between above studies in the autocrine inhibitory effect of IL-10 on IL-12 p40 production may be attributable to the differences in cell types and/or culture conditions such as cell density and stimuli.

We performed the blocking study using anti-TNF-α mAb (clone: MP6-XT22), anti-TNFR1 mAb (clone: 55R-170), and anti-TNFR2 mAb (clone: TR75-54.7). TNF-α-induced increase in CD86 expression on BC1 cells [35] was completely inhibited by treatment with the anti-TNFR1 mAb or the anti-TNF-α mAb (data not shown). However, these mAbs failed to exert significant effects on the IL-10 production by DCs upon the TLR stimulation (data not shown). As a possible explanation for the discrepant results, attenuated TNF-α signal in the presence of the mAb might be enough to enhance the TLR-mediated IL-10 production. Alternatively, a constitutive weak TNF-α signaling before the antibody treatment might be sufficient to facilitate IL-10 production upon TLR stimulation.

We also analyzed production of IL-23, a member of the IL-12 cytokine family, in WT and TNF-$\alpha^{-/-}$ DCs upon TLR stimulation. TLR ligands induced substantial production of IL-23 in WT and TNF-$\alpha^{-/-}$ DCs. The IL-23 production by TNF-$\alpha^{-/-}$ DCs was higher than that by WT DCs (data not shown). In contrast, the IL-12 p40 production upon the TLR stimulation slightly decreased in TNF-$\alpha^{-/-}$ DCs compared to WT DCs (Fig. 1). Thus, the level of IL-12 p40 production did not reflect to that of IL-23 production in our culture system. It has been shown that IL-12 p40 expression was not parallel to IL-23 p19 expression in DCs [44]. It seems to us that this point should be carefully analyzed in future studies.

We demonstrated herein that TNF-α signaling to promote DC production of anti-inflammatory cytokine, IL-10, but not inflammatory cytokine, IL-12, upon TLR stimulation. Thus, TNF-α may be a key molecule to regulate the balance between anti-inflammatory versus inflammatory cytokines in DCs. However, the precise mechanism underlying the TNF-α-mediated regulation of IL-10 production remains to be unclear. Thus, we would like to identify the molecular mechanisms responsible for the TNF-α-mediated regulation system in the future studies. Since the balance between IL-10 and IL-12 production by DCs is crucial to induce appropriate immune responses, further elucidation of the TNF-α-mediated immune regulation may lead to the development of clinical applications for the treatment of various immune disorders.

Acknowledgments

This study was supported in part by a Grant-in-Aid for Scientific Research (B) from the Japan Society for the Promotion of Science (JSPS), Global COE Program 'Establishment of International Collaboration Center for Zoonosis Control' from Ministry of Education, Japan.

References

[1] B.B. Aggrawal, Signalling pathways of the TNF superfamily: a double-edged sword, Nat. Rev. Immunol. 3 (2003) 745–756.
[2] F. Balkwill, Tumour necrosis factor and cancer, Nat. Rev. Cancer 9 (2009) 361–371.
[3] P. Vandenabeele, W. Declercq, R. Beyaert, W. Fiers, Two tumour necrosis factor receptors: structure and function, Trends Cell Biol. 5 (1995) 392–399.
[4] V. Baud, M. Karin, Signal transduction by tumor necrosis factor and its relatives, Trends Cell Biol. 11 (2001) 372–377.
[5] B.W. Winston, D.W. Riches, Activation of $p42^{mapk/erk2}$ following engagement of tumor necrosis factor receptor CD120a (p55) in mouse macrophages, J. Immunol. 155 (1995) 1525–1533.
[6] H. Wajant, K. Pfizenmaier, P. Scheurich, Tumor necrosis factor signaling, Cell Death Differ. 10 (2003) 45–65.
[7] I.E. Wertz, V.M. Dixit, Ubiquitin-mediated regulation of TNFR1 signaling, Cytokine Growth Factor Rev. 19 (2008) 313–324.
[8] T. Kawai, S. Akira, Pathogen recognition with Toll-like receptors, Curr. Opin. Immunol. 17 (2005) 338–344.
[9] J.L. Imler, J.A. Hoffmann, Toll signaling: the TIReless quest for specificity, Nat. Immunol. 4 (2003) 105–106.
[10] L.A. O'Neill, A.G. Bowie, The family of five: TIR-domain-containing adaptors in Toll-like receptor signaling, Nat. Rev. Immunol. 7 (2007) 353–364.
[11] R. Medzhitov, P. Preston-Hurlburt, E. Kopp, A. Stadlen, C. Chen, S. Ghosh, C.A.J. Janeway, MyD88 is an adaptor protein in the hToll/IL-1 receptor family signaling pathways, Mol. Cell 2 (1998) 253–258.
[12] S. Akira, K. Takeda, T. Kaisho, Toll-like receptors: critical proteins linking innate and acquired immunity, Nat. Immunol. 2 (2001) 675–680.
[13] K.A. Fitzgerald, E.M. Palsson-McDermott, A.G. Bowie, C.A. Jefferies, A.S. Mansell, G. Brady, E. Brint, A. Dunne, P. Gray, M.T. Harte, D. McMurray, D.E. Smith, J.E. Sims, T.A. Bird, L.A. O'Neill, Mal (MyD88-adapter-like) is required for Toll-like receptor-4 signal transduction, Nature 413 (2001) 78–83.
[14] T. Horng, G.M. Barton, R. Medzhitov, Tirap: an adapter molecule in the Toll signaling pathway, Nat. Immunol. 2 (2001) 835–841.
[15] M.W. Covert, T.H. Leung, J.E. Gaston, D. Baltimore, Achieving stability of lipopolysaccharide-induced NF-κB activation, Science 309 (2005) 1854–1857.
[16] T. Kawai, S. Akira, Signaling to NF-κB by Toll-like receptors, Trends Mol. Med. 13 (2007) 460–469.
[17] W.L. Yang, J. Wang, C.H. Chan, S.W. Lee, A.D. Campos, B. Lamothe, L. Hur, B.C. Grabiner, X. Lin, B.G. Darnay, H.K. Lin, The E3 ligase TRAF6 regulates Akt ubiquitination and activation, Science 325 (2009) 1134–1138.
[18] S.S. Sierra, S.D. Deshmukh, J. Kalnitski, P. Küenzi, M.P. Wymann, D.T. Golenbock, P. Henneke, Mal connects TLR2 to PI3Kinase activation and phagocyte polarization, EMBO J. 28 (2009) 2018–2027.
[19] M.H. Laird, S.H. Rhee, D.J. Perkins, A.E. Medvedev, W. Piao, M.J. Fenton, S.N. Vogel, TLR4/MyD88/PI3K interactions regulate TLR4 signaling, J. Leukoc. Biol. 85 (2009) 966–977.

[20] R.M. Steinman, The dendritic cell system and its role in immunogenicity, Annu. Rev. Immunol. 9 (1991) 271–296.
[21] D.N.J. Hart, Dendritic cells: unique leukocyte populations which control the primary immune response, Blood 90 (1997) 3245–3287.
[22] J. Banchereau, R.M. Steinman, Dendritic cells and the control of immunity, Nature 392 (1998) 245–251.
[23] P. McGuirk, K.H. Mills, Pathogen-specific regulatory T cells provoke a shift in the Th1/Th2 paradigm in immunity to infectious diseases, Trends Immunol. 23 (2002) 450–455.
[24] S. Rutella, S. Danese, G. Leone, Tolerogenic dendritic cells: cytokine modulation comes of age, Blood 108 (2006) 1435–1440.
[25] Y. Belkaid, Regulatory T cells and infection: a dangerous necessity, Nat. Rev. Immunol. 7 (2007) 875–888.
[26] A. O'Garra, P. Vieira, Th1 cells control themselves by producing interleukin-10, Nat. Rev. Immunol. 7 (2007) 425–428.
[27] J. Hodge-Dufour, M.W. Marino, M.R. Horton, A. Jungbluth, M.D. Burdick, R.M. Strieter, P.W. Noble, C.A. Hunter, E. Puré, Inhibition of interferon γ induced interleukin 12 production: a potential mechanism for the anti-inflammatory activities of tumor necrosis factor, Proc. Natl. Acad. Sci. USA 95 (1998) 13806–13811.
[28] X. Ma, J. Sun, E. Papasavvas, H. Riemann, S. Robertson, J. Marshall, R.T. Bailer, A. Moore, R.P. Donnelly, G. Trinchieri, L.J. Montaner, Inhibition of IL-12 production in human monocyte-derived macrophages by TNF, J. Immunol. 164 (2000) 1722–1729.
[29] M. Zakharova, H.K. Ziegler, Paradoxical anti-inflammatory actions of TNF-α: inhibition of IL-12 and IL-23 via TNF receptor 1 in macrophages and dendritic cells, J. Immunol. 175 (2005) 5024–5033.
[30] C. Wanidworanun, W. Strober, Predominant role of tumor necrosis factor-α in human monocyte IL-10 synthesis, J. Immunol. 151 (1993) 6853–6861.
[31] S.L. Parry, M. Sebbag, M. Feldmann, F.M. Brennan, Contact with T cells modulates monocyte IL-10 production, J. Immunol. 158 (1997) 3673–3681.
[32] K. Inaba, M. Inaba, N. Romani, H. Aya, M. Deguchi, S. Ikehara, S. Muramatsu, R.M. Steinman, Generation of large numbers of dendritic cells from mouse bone marrow cultures supplemented with granulocyte/macrophage colony-stimulating factor, J. Exp. Med. 176 (1992) 1693–1702.
[33] S. Yamazaki, A.J. Bonito, R. Spisek, M. Dhodapkar, K. Inaba, R.M. Steinman, Dendritic cells are specialized accessory cells along with TGF-β for the differentiation of Foxp3$^+$ CD4$^+$ regulatory T cells from peripheral Foxp3 precursors, Blood 110 (2007) 4293–4302.
[34] N. Hirata, Y. Yanagawa, T. Ebihara, T. Seya, S. Uematsu, S. Akira, F. Hayashi, K. Iwabuchi, K. Onoé, Selective synergy in anti-inflammatory cytokine production upon cooperated signaling via TLR4 and TLR2 in murine conventional dendritic cells, Mol. Immunol. 45 (2008) 2734–2742.
[35] Y. Yanagawa, N. Iijima, K. Iwabuchi, K. Onoé, Activation of extracellular signal-related kinase by TNF-α controls the maturation and function of murine dendritic cells, J. Leukoc. Biol. 71 (2002) 125–132.
[36] S.M. Mäkelä, M. Strengell, T.E. Pietilä, P. Österlund, I. Julkunen, Multiple signaling pathways contribute to synergistic TLR ligand-dependent cytokine gene expression in human monocyte-derived macrophages and dendritic cells, J. Leukoc. Biol. 85 (2009) 664–672.
[37] R. Pincheira, A.F. Castro, O.N. Ozes, P.S. Idumalla, D.B. Donner, Type 1 TNF receptor forms a complex with and uses Jak2 and c-Src to selectively engage signaling pathways that regulate transcription factor activity, J. Immunol. 181 (2008) 1288–1298.
[38] M.A. Rivas, R.P. Carnevale, C.J. Proietti, C. Rosemblit, W. Beguelin, M. Salatino, E.H. Charreau, I. Frahm, S. Sapia, P. Brouckaert, P.V. Elizalde, R. Schillaci, TNFα acting on TNFR1 promotes breast cancer growth via p42/P44 MAPK, JNK, Akt and NF-κB-dependent pathways, Exp. Cell Res. 314 (2008) 509–529.
[39] Y.W. Liu, C.C. Chen, H.P. Tseng, W.C. Chang, Lipopolysaccharide-induced transcriptional activation of interleukin-10 is mediated by MAPK- and NF-κB-induced CCAAT/enhancer-binding protein δ in mouse macrophages, Cell Signal. 18 (2006) 1492–1500.
[40] O. Norkina, A. Dolganiuc, T. Shapiro, K. Kodys, P. Mandrekar, G. Szabo, Acute alcohol activates STAT3, AP-1, and Sp-1 transcription factors via the family of Src kinases to promote IL-10 production in human monocytes, J. Leukoc. Biol. 82 (2007) 752–762.
[41] M.S. Vivarelli, D. McDonald, M. Miller, N. Cusson, M. Kelliher, R.S. Geha, RIP links TLR4 to Akt and is essential for cell survival in response to LPS stimulation, J. Exp. Med. 200 (2004) 399–404.
[42] K. Saegusa, S. Yotsumoto, S. Kato, Y. Aramaki, Phosphatidylinositol 3-kinase-mediated regulation of IL-10 and IL-12 production in macrophages stimulated with CpG oligodeoxynucleotide, Mol. Immunol. 44 (2007) 1323–1330.
[43] M. Ohtani, S. Nagai, S. Kondo, S. Mizuno, K. Nakamura, M. Tanabe, T. Takeuchi, S. Matsuda, S. Koyasu, Mammalian target of rapamycin and glycogen synthase kinase 3 differentially regulate lipopolysaccharide-induced interleukin-12 production in dendritic cells, Blood 112 (2008) 635–643.
[44] F. Gerosa, B. Baldani-Guerra, L.A. Lyakh, G. Batoni, S. Esin, R.T. Winkler-Pickett, M.R. Consolaro, M. De Marchi, D. Giachino, A. Robbiano, M. Astegiano, A. Sambataro, R.A. Kastelein, G. Carra, G. Trinchieri, Differential regulation of interleukin 12 and interleukin 23 production in human dendritic cells, J. Exp. Med. 205 (2008) 1447–1461.

Cell Mol Neurobiol (2011) 31:1009–1020
DOI 10.1007/s10571-011-9698-x

ORIGINAL RESEARCH

Non-phosphorylated FTY720 Induces Apoptosis of Human Microglia by Activating SREBP2

Takashi Yoshino · Hiroko Tabunoki · Shigeo Sugiyama · Keitaro Ishii · Seung U. Kim · Jun-ichi Satoh

Received: 3 February 2011 / Accepted: 14 April 2011 / Published online: 26 April 2011

Abstract A synthetic analog of sphingosine named FTY720 (Fingolimod), phosphorylated by sphingosine kinase-2, interacts with sphingosine-1-phosphate (S1P) receptors expressed on various cells. FTY720 suppresses the disease activity of multiple sclerosis (MS) chiefly by inhibiting S1P-dependent egress of autoreactive T lymphocytes from secondary lymphoid organs, and possibly by exerting anti-inflammatory and neuroprotective effects directly on brain cells. However, at present, biological effects of FTY720 on human microglia are largely unknown. We studied FTY720-mediated apoptosis of a human microglia cell line HMO6. The exposure of HMO6 cells to non-phosphorylated FTY720 (FTY720-non-P) induced apoptosis in a dose-dependent manner with IC50 of 10.6 ± 2.0 μM, accompanied by the cleavage of caspase-7 and caspase-3 but not of caspase-9. The apoptosis was inhibited by Z-DQMD-FMK, a caspase-3 inhibitor, but not by Pertussis toxin, a Gi protein inhibitor, suramin, a S1P3/S1P5 inhibitor, or W123, a S1P1 competitive antagonist, although HMO6 expressed S1P1, S1P2, and S1P3. Furthermore, both phosphorylated FTY720 (FTY720-P) and SEW2871, S1P1 selective agonists, did not induce apoptosis of HMO6. Genome-wide gene expression profiling and molecular network analysis indicated activation of transcriptional regulation by sterol regulatory element-binding protein (SREBP) in FTY720-non-P-treated HMO6 cells. Western blot verified activation of SREBP2 in these cells, and apoptosis was enhanced by pretreatment with simvastatin, an activator of SREBP2, and by overexpression of the N-terminal fragment of SREBP2. These observations suggest that FTY720-non-P-induced apoptosis of HMO6 human microglia is independent of S1P receptor binding, and positively regulated by the SREBP2-dependent proapoptotic signaling pathway.

Keywords Apoptosis · Cholesterol · FTY720 · Microglia · S1P1 · SREBP2

Abbreviations

CNS	Central nervous system
DAVID	Database for Annotation, Visualization, and Integrated Discovery
EDG	Endothelial differentiation gene
FTY720-non-P	Non-phosphorylated form of FTY720
FTY720-P	Phosphorylated form of FTY720
G3PDH	Glyceraldehyde-3-phosphate dehydrogenase
GPCR	G-protein-coupled receptor
INSIG1	Insulin-induced gene 1
LDLR	Low density lipoprotein receptor

Electronic supplementary material The online version of this article (doi:10.1007/s10571-011-9698-x) contains supplementary material, which is available to authorized users.

T. Yoshino · H. Tabunoki · J. Satoh (✉)
Department of Bioinformatics and Molecular Neuropathology, Meiji Pharmaceutical University, 2-522-1 Noshio, Kiyose, Tokyo 204-8588, Japan
e-mail: satoj@my-pharm.ac.jp

S. Sugiyama · K. Ishii
Department of Chemistry of Functional Molecules, Meiji Pharmaceutical University, 2-522-1 Noshio, Kiyose, Tokyo 204-8588, Japan

S. U. Kim
Division of Neurology, Department of Medicine, University of British Columbia Hospital, University of British Columbia, Vancouver, BC, Canada

S. U. Kim
Medical Research Institute, Chung-Ang University College of Medicine, Seoul, Korea

MS	Multiple sclerosis
OPC	Oligodendroglial progenitor cell
S1P	Sphingosine-1-phosphate
SPHK2	Sphingosine kinase-2
SREBP	Sterol regulatory element-binding protein
PARP	Poly-ADP-ribose-polymerase
PTX	Pertussis toxin

Introduction

FTY720 (Fingolimod) is a synthetic analog of sphingosine generated by chemical modification of myriocin, a natural product of the fungus *Isaria sinclairii*. FTY720, phosphorylated by endogenous sphingosine kinase-2 (SPHK2), is converted into the biologically active form FTY720-P that binds to sphingosine-1-phosphate (S1P) receptors expressed on various cells (Brinkmann et al. 2010). S1P receptors belong to the endothelial differentiation gene (EDG) receptor family of G-protein-coupled receptors (GPCRs). FTY720-P interacts with S1P1, S1P3, S1P4, and S1P5 but not with S1P2. S1P1, S1P2, and S1P3 are distributed widely in the immune system, cardiovascular system, and the central nervous system (CNS), and S1P4 expression is more restricted to the lung, spleen, and thymus, while S1P5 is located chiefly on the skin, spleen, and brain. FTY720-P not only serves as an agonist for S1P receptors, but also acts as a functional antagonist for S1P1 by downregulating the receptor expression via internalization, ubiquitination, and proteasomal degradation (Mullershausen et al. 2009). The latter induces unresponsiveness to endogenous S1P.

Recent clinical trials indicate that FTY720 has promising therapeutic effects on multiple sclerosis (MS), a human demyelinating disease affecting exclusively the CNS white matter (Brinkmann et al. 2010). Oral administration of FTY720 reduces the number of gadolinium-enhanced lesions on MRI and decreased annual relapse rate in the patients with relapsing-remitting MS (Kappos et al. 2006). Consequently, US Food and Drug Administration (FDA) approved FTY720 as the first oral medication for MS in September 2010. FTY720-mediated immunomodulatory effects on the disease activity of MS are chiefly attributable to inhibition of S1P-dependent egress of autoreactive T lymphocytes from secondary lymphoid organs (Brinkmann et al. 2010).

Increasing evidence indicates that FTY720, capable of passing the blood–brain barrier due to its lipophilicity, exerts anti-inflammatory and neuroprotective effects within the CNS by interacting with a battery of S1P receptors expressed on neural cells (Dev et al. 2008). Reactive astrocytes in active MS lesions show a robust increase in S1P1 and S1P3 expression, where FTY720-P inhibits production of proinflammatory cytokines from astrocytes (Van Doorn et al. 2010). FTY720-P persistently downregulates S1P1 expression on astrocytes, and thereby attenuates the disease activity of experimental autoimmune encephalomyelitis (EAE), an animal model of MS (Choi et al. 2011). FTY720-P induces rapid phosphorylation of ERK1/2 and activates the PI3-kinase/Akt pathway in rat oligodendrocyte progenitor cells (OPCs), and subsequently protects OPCs from apoptosis caused by proinflammatory mediators (Coelho et al. 2007). FTY720-P promotes process extension of human OPCs and enhances their survival (Miron et al. 2008).

Microglia, acting as antigen-presenting cells and proinflammatory effector cells in the CNS, play a central role in development of demyelinating lesions in MS (Jack et al. 2005). Therefore, it is possible that FTY720 acts directly on microglia at the site of inflammation in MS brains. S1P1-expressing cells positive for CD68, a marker of microglia/macrophages, are accumulated in MS lesions (Van Doorn et al. 2010). Rat microglial cells express mainly S1P1 and S1P3 (Dev et al. 2008). In mouse organotypic cerebellar cultures affected with lysolecithin-induced demyelination, FTY720-P induces proliferation of microglia (Miron et al. 2010), while FTY720 reduces the accumulation of reactive microglia/macrophages in the lesions of traumatic brain injury (Zhang et al. 2007). FTY720 reduces the lesion size of cerebral infarct in mice with middle cerebral artery (MCA) occlusion and improves neurological deficits, accompanied by a decrease in the number of activated microglia/macrophages and apoptotic neurons (Wei et al. 2011). FTY720-P does not affect the global cytokine production by cultured human microglia (Durafourt et al. 2011). However, at present, immunomodulatory effects of FTY720 on human microglia remain largely unknown. The aim of the present study is to investigate biological effects of FTY720 on a human microglial cell line HMO6.

Methods

Human Microglia Cell Line HMO6

The HMO6 cell line was established by immortalizing cultured microglia isolated from human embryonic telencephalon tissues with a retroviral vector PASK1.2 encoding v-myc oncogene (Nagai et al. 2001). HMO6 cells express the markers of the microglia/macrophage lineage cells, including CD11b, CD68, CD86, HLA-ABC, HLA-DR, and ricinus communis agglutinin lectin-1 (RCA), serving as a model of human microglia both in

vitro and in vivo (Narantuya et al. 2010). The cells were maintained in Dulbecco's Modified Eagle's medium (DMEM; Invitrogen, Carlsbad, CA, USA) supplemented with 10% fetal bovine serum (FBS), 100 U/ml penicillin and 100 μg/ml streptomycin (feeding medium). Human neural and non-neural cell lines other than HMO6 were described elsewhere. LDH release from cultured cells was assessed by using a LDH cytotoxicity detection kit (Takara Bio, Shiga, Japan).

Chemicals

Non-phosphorylated FTY720 (FTY720-non-P; Calbiochem, Darmstadt, Germany) and *(S)*-FTY720 phosphate (FTY720-P; Echelon Biosciences, Salt Lake City, UT, USA) were usually dissolved in dimethyl sulfoxide (DMSO), providing the stock solution at the concentration of 10 mM. For negative controls, the inclusion of DMSO at the concentration of 0.1% v/v (1:1000 dilution) was applied. We found that the solvent alone never induces apoptosis of HMO6 at any incubation time. Sphingosine 1-phosphate (S1P) was obtained form Sigma, St. Louis, MO, USA. SEW2871, a selective S1P1 agonist and W123, a competitive S1P1 antagonist were obtained from Cayman Chemical, Ann Arbor, MI, USA. Suramin, a S1P3/S1P5 inhibitor, Z-DQMD-FMK, a caspase-3 inhibitor, and simvastatin, a HMG-CoA reductase inhibitor were obtained from Calbiochem. Pertussis toxin (PTX), a Gi protein inhibitor, was obtained form Seikagaku Biobusiness, Tokyo, Japan.

RT-PCR Analysis

Total cellular RNA was extracted by using TRIZOL (Invitrogen). RNA treated with DNase I was processed for cDNA synthesis using oligo$(dT)_{20}$ primers and SuperScript II reverse transcriptase (Invitrogen). Then, cDNA was amplified by PCR using HotStar Taq DNA polymerase (Qiagen, Valencia, CA, USA) and a panel of sense and antisense primer sets following: 5′aagcgctctttacttggtcgc tgg3′ and 5′tgatctccacccttcccagtgcat3′ for an 189 bp product of S1P1; 5′ccacagacctgggtgatgttg3′ and 5′tccccttaaatgctgcc tgcc3′ for a 200 bp product of S1P2; 5′actttgggctccagagtct ttc3′ and 5′cattctacgcacaggaaatgtagtg3′ for an 193 bp product of S1P3; 5′gttgcagtcttgcgtgtggatgg3′ and 5′ggtgac catgggaagcccatttg3′ for an 183 bp product of S1P4; 5′aggaatggcatgcgcaaag3′ and 5′cttctatggctcccacctcactc3′ for a 200 bp product of S1P5; and 5′ccatgttcgtcatgggtgtgaacca3′ and 5′gccagtagaggcagggatgatgttc3′ for a 251 bp product of the glyceraldehyde-3-phosphate dehydrogenase (G3PDH) gene.

For quantitative real-time RT-PCR (qPCR) analysis, cDNA was amplified by PCR in LightCycler ST300 (Roche Diagnostics, Tokyo, Japan) using SYBR Green I and a panel of sense and antisense primer sets with the following: 5′tgatcgttccagaagtggccttgg3′ and 5′aactgtcgtc ctatgttccccacc3′ for an 186 bp product of insulin-induced gene 1 (INSIG1) and 5′ctgggggtcttccttctatggaag3′ and 5′cacgtcatcctccagactgaccat3′ for an 168 bp product of low density lipoprotein receptor (LDLR). The expression levels of target genes were standardized against the levels of G3PDH, an internal control, detected in corresponding cDNA samples. All the assays were performed in triplicate.

Microarray Analysis

For microarray analysis, total cellular RNA was isolated by using the TRIZOL Plus RNA Purification kit (Invitrogen). The quality of total RNA was evaluated on Agilent 2100 Bioanalyzer (Agilent Technologies, Palo Alto, CA, USA). One hundred ng of total RNA was processed for cRNA synthesis, fragmentation, and terminal labeling with the GeneChip Whole Transcript Sense Target Labeling and Control Reagents (Affymetrix, Santa Clara, CA, USA). Then, it was processed for hybridization at 45°C for 17 h with Human Gene 1.0 ST Array that contains 28,869 genes (Affymetrix). The arrays were washed in the GeneChip Fluidic Station 450 (Affymetrix), and scanned by the GeneChip Scanner 3000 7G (Affymetrix). The raw data were expressed as CEL files and normalized by the robust multiarray average (RMA) method with the Expression Console software version 1.1 (Affymetrix). The annotation was studied by searching genes on the Database for Annotation, Visualization, and Integrated Discovery (DAVID) (david.abcc.ncifcrf.gov) (da Huang et al. 2009).

Molecular Network Analysis

KeyMolnet is a comprehensive knowledgebase that contains the contents on 123,000 relationships among human genes and proteins, small molecules, diseases, pathways and drugs, regularly updated, and curated by expert biologists (Satoh et al. 2009). By importing the list of Entrez Gene IDs derived from microarray data, KeyMolnet automatically provides corresponding molecules as a node on networks. Among various network-searching algorithms, the "neighboring" network-search algorithm selected one or more molecules as starting points to generate the network of all kinds of molecular interactions around starting molecules, including direct activation/inactivation, transcriptional activation/repression, and the complex formation within the designated number of paths from starting points. The generated network was compared side by side with 430 human canonical pathways of the KeyMolnet library. The algorithm counting the number of overlapping molecular relations between the extracted network and the

canonical pathway makes it possible to identify the canonical pathway showing the most significant contribution to the extracted network. The significance in the similarity between both is scored following the formula, where O = the number of overlapping molecular relations between the extracted network and the canonical pathway, V = the number of molecular relations located in the extracted network, C = the number of molecular relations located in the canonical pathway, T = the number of total molecular relations, and the X = the sigma variable that defines coincidence.

$$\text{Score} = -\log_2(\text{Score(p)}) \quad \text{Score (p)} = \sum_{x=O}^{Min(C,V)} f(x)$$

$$f(x) = {}_{C}C_{x} \cdot {}_{T-C}C_{V-x} / {}_{T}C_{V}$$

Transient Expression of SREBP2

To transiently overexpress sterol regulatory element-binding protein-2 (SREBP2), the gene encoding the N-terminal fragment of SREBP2 spanning amino acid residues 1–484 was amplified by PCR using PfuTurbo DNA polymerase (Stratagene, La Jolla, CA) and a sense and antisense primer set of 5′gcgatggacgacagcggcgagctg3′ and 5′tcacagaagaatccg tgagcggtc3′, and cloned in the expression vector pEF6 (Invitrogen). The vector was transfected into HMO6 cells by X-tremeGENE HP DNA transfection reagent (Roche Diagnostics). At 24 h after transfection, the cells were processed for western blot analysis. For the control, V5-tagged LacZ cloned in the pEF6 vector was transfected into sister cultures.

Western Blot Analysis

To prepare total protein extract, the cells were homogenized in RIPA buffer supplemented with a cocktail of protease inhibitors (Sigma). The protein extract was centrifuged at 12,000 rpm for 5 min at room temperature (RT). The protein concentration was determined by a Bradford assay kit (BioRad Hercules, CA, USA). The mixture of the supernatant and a 2× Lammeli loading buffer was boiled and separated on SDS-PAGE gels ranging from 8 to 12%. After gel electrophoresis, the protein was transferred onto nitrocellulose membranes, and immunolabeled at RT overnight with rabbit anti-poly-ADP-ribose-polymerase (PARP) antibody (#11835238001; Roche Diagnostics), rabbit anti-cleaved caspase-3 (Asp175) antibody (#9661; Cell Signaling Technology, Danvers, MA, USA), mouse anti-caspase-7 antibody (#9494; Cell Signaling Technology), rabbit anti-caspase-9 antibody (#9502; Cell Signaling Technology), rabbit anti-S1P1 antibody (sc-25489, EDG-1, H-60; Santa Cruz Biotechnology, Santa Cruz, CA), or goat anti-SREBP2 antibody (sc-8151, N-19; Santa Cruz Biotechnology). Then, the membranes were incubated at RT for 60 min with HRP-conjugated anti-mouse IgG, anti-rabbit IgG, or anti-goat IgG (Santa Cruz Biotechnology). The specific reaction was visualized by exposing the membranes to a chemiluminescent substrate (Thermo Scientific, Rockford, IL, USA).

In some experiments, the antibodies were stripped by incubating the membranes at 50°C for 30 min in stripping buffer, composed of 62.5 mM Tris-HCl, pH 6.7, 2% SDS, and 100 mM 2-mercaptoethanol. Then, the membranes were processed for relabeling with goat anti-heat shock protein HSP60 antibody (sc-1052, N-20; Santa Cruz Biotechnology) used for an internal control of protein loading, followed by incubation with HRP-conjugated anti-goat IgG.

Results

S1P Receptor Expression on Human Microglia Cell Line HMO6

The expression of five S1P receptor mRNAs in a panel of human neural cells and tissues was determined by RT-PCR. All the cells and tissues examined, including the human cerebrum (CBR), fetal astrocytes (AS), neuronal progenitor (NP) cells, NTera2 teratocarcinoma-derived neurons, SK-N-SH neuroblastoma, IMR-32 neuroblastoma, U-373MG astroglioma, and the microglia cell line HMO6, expressed varying levels of S1P1, S1P2, and S1P3 mRNAs, except for Y79 retinoblastoma that did not express S1P1 (Fig. 1a–c, lanes 2–10). In contrast, the levels of G3PDH, a housekeeping gene, were almost constant in the cells and tissues examined (Fig. 1f, lanes 2–10). Although discernible levels of S1P4 and S1P5 mRNAs were identified in the human cerebrum (CBR), both of these mRNAs were almost undetectable in HMO6 (Fig. 1d, e, lanes 2 and 10). No products were amplified when the reverse transcription step is omitted (Fig. 1a–f, lane 1). We verified S1P1 protein expression in HMO6 by western blot (not shown).

Non-Phosphorylated FTY720 Induced Apoptosis of HMO6

A 6 h-exposure of non-phosphorylated FTY720 (FTY720-non-P) induced LDH release from HMO6 cells and cell death in a dose-dependent manner with IC50 of 10.6 ± 2.0 μM (Fig. 2a, c). It is worthy to note that the concentration of FTY720-non-P at lower than 5 μM was completely ineffective in inducing cell death of HMO6 (Fig. 2a). Generally, LDH release did not discriminate apoptotic and necrotic cell death. The exposure of FTY720-non-P at a concentration of 10 μM mediated the cleavage of PARP in the incubation time longer than 4 h,

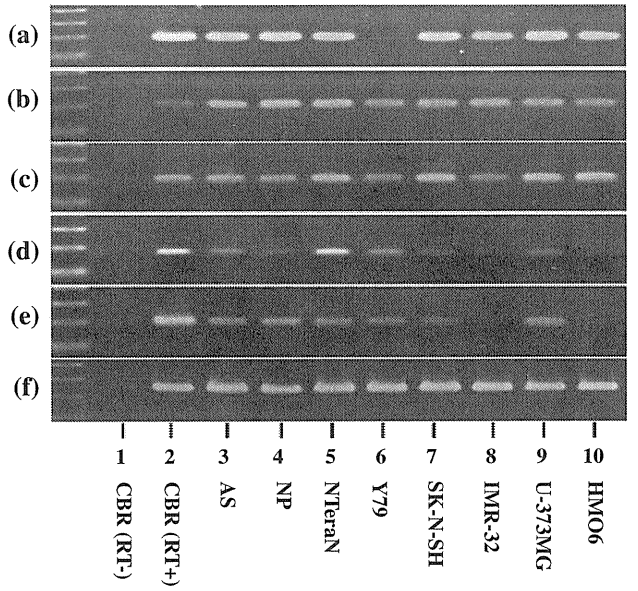

Fig. 1 S1P receptor expression in human neural cell lines. The expression of five S1P receptor mRNAs was studied by RT-PCR. **a** S1P1, **b** S1P2, **c** S1P3, **d** S1P4, **e** S1P5, and **f** G3PDH. The lanes (*1–10*) represent (*1*) the human frontal cerebral cortex (CBR) without inclusion of the reverse transcription (RT) step, (*2*) CBR with inclusion of the RT step, (*3*) cultured astrocytes (AS), (*4*) cultured neuronal progenitor (NP) cells, (*5*) NTera2 teratocarcinoma-derived neurons (NTera2N), (*6*) Y79 retinoblastoma, (*7*) SK-N-SH neuroblastoma, (*8*) IMR-32 neuroblastoma, (*9*) U-373MG astrocytoma, and (*10*) HMO6 microglia. The 100 bp ladder marker is shown on the left

indicating that FTY720-non-P induced cell death of HMO6 via apoptosis (Fig. 2d, lanes 7–10).

FTY720-non-P-induced apoptosis of HMO6 was accompanied by the cleavage of caspase-7 and caspase-3 (Fig. 3b, c, lane 2) but not of caspase-9 (Fig. 3e, lane 4), suggesting that the mitochondrial pathway of apoptosis that usually activates caspase-9 did not play a major role. Furthermore, Z-DQMD-FMK, a caspase-3-specific inhibitor, completely blocked FTY720-non-P-induced apoptosis of HMO6 (Fig. 3g, h, lane 10).

FTY720-Induced Apoptosis of HMO6 was Independent of S1P Receptor Binding

Because FTY720, when phosphorylated, binds to S1P1, S1P3, S1P4, and S1P5, all of which are G protein-coupled receptors (GPCR), we utilized Pertussis toxin (PTX), a Gi protein inhibitor, suramin, a S1P3/S1P5 inhibitor, and W123, a S1P1 competitive antagonist to block the ligand-receptor interaction. However, none of these receptor blockers could inhibit FTY720-induced apoptosis of HMO6 (Fig. 4a, lanes 4, 6, 8). Furthermore, SEW2871, a S1P1 selective agonist, and phosphorylated FTY720 (FTY720-P) at a concentration of 10 μM each did not induce apoptosis of HMO6 during the incubation time of 12 h (Fig. 4c, lanes 11 and 12). In addition, the combined administration of FTY720-P (10 μM) and FTY720-non-P (10 μM) did not inhibit apoptosis of HMO6, and treatment with sphiongosine-1 phosphate (S1P) (10–50 μM) did not induce apoptosis of HMO6 (data not shown). These results suggest that FTY720-non-P-induced apoptosis of HMO6 was independent of S1P receptor binding, and both FTY720-P and S1P were incapable of inducing apoptosis of HMO6.

FTY720 Induced SREBP-Responsive Genes

To investigate the molecular mechanism responsible for triggering FTY720-non-P-induced apoptosis of HMO6, we studied the genome-wide gene expression profile by microarray analysis. We identified 30 genes with an over 2-fold increase in HMO6 cells treated for 2 h with 10 μM FTY720-non-P versus those exposed to the vehicle (DMSO) (Table 1). Among them, the DAVID program categorized seven genes as a group of the genes associated with steroid and/or sterol metabolism (Table 1). None of apoptosis initiator and executor genes were induced in HMO6 cells at 2 h after initiation of the treatment. Upregulated expression of INSIG1 and LDLR in FTY720-non-P-treated HMO6 cells was validated by qPCR analysis (Fig. 5a, b).

Next, we imported the list of Entrez Gene IDs of the 30 genes upregulated in FTY720-non-P-treated HMO6 cells into KeyMolnet, a tool for analyzing molecular interactions on the comprehensive knowledgebase. KeyMolnet generated the molecular network, presenting with the most significant relationship with transcriptional regulation by sterol regulatory element-binding protein (SREBP) (the score = 69.719 with the *P*-value = 1.029E−21) (Fig. 5c). These results suggest that in HMO6 cells, FTY720-non-P activates SREBP proteins, either SREBP1 or SREBP2, belonging to the bHLH-Zip transcription factor family that promotes the synthesis of enzymes involved in cholesterol and fatty acid biosynthesis. To exclude a direct effect of vehicle (DMSO), in which FTY720-non-P was dissolved, on gene expression, we performed an additional set of microarray experiment by exposing HMO6 cells to FTY720-non-P dissolved in ethanol. We again identified the similar gene expression profile composed of upregulation of key SREBP-target genes, regardless of the solvent (See Table 1 in Electronic Supplementary Material).

SREBP2 is primarily involved in cholesterol synthesis, while SREBP1 chiefly regulates fatty acid synthesis (Sato 2010). INSIG1 identified by microarray analysis encodes an ER protein that plays a pivotal role in regulating intracellular cholesterol levels by interacting with SREBP cleavage-activating protein (SCAP) having the sterol-sensing domain activated by reduced cellular cholesterol levels. Thereafter, we have focused on SREBP2 expression

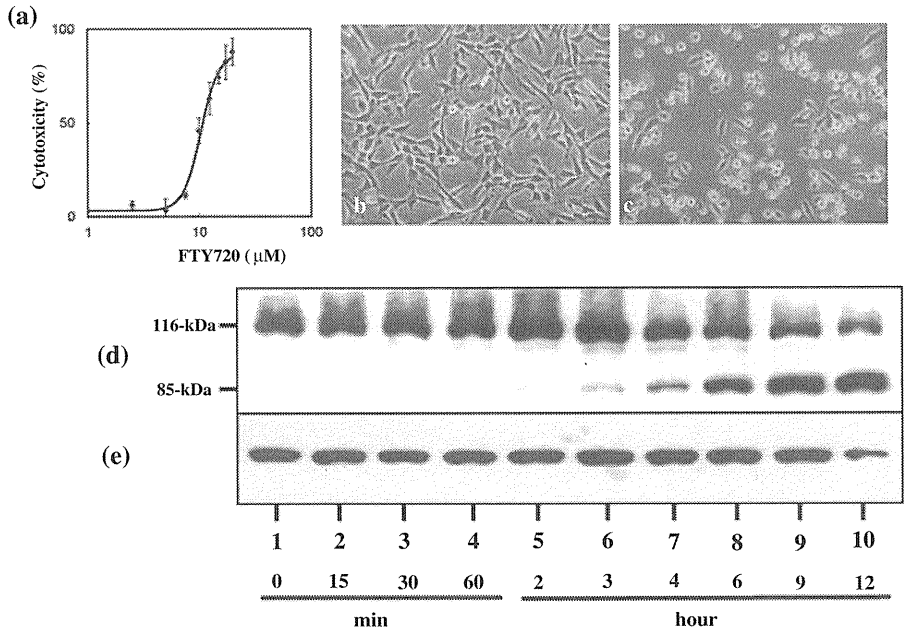

Fig. 2 Non-phosphorylated FTY720 induced apoptosis of HMO6 cells. HMO6 cells were exposed for various time periods to varying concentrations of non-phosphorylated FTY720 (FTY720-non-P). **a** LDH release assay, **b** the phase contrast photomicrograph of the cells exposed for 6 h to vehicle (DMSO), **c** the phase contrast photomicrograph of the cells exposed for 6 h to 10 μM FTY720-non-P, **d** western blot of PARP (an 116-kDa uncleaved form and an 85-kDa cleaved form), and **e** western blot of HSP60, an internal control of protein loading. The lanes (*1–10*) represent (*1*) untreated HMO6 cells, and HMO6 cells treated for (*2*) 15 min, (*3*) 30 min, (*4*) 1 h, (*5*) 2 h, (*6*) 3 h, (*7*) 4 h, (*8*) 6 h, (*9*) 9 h, and (*10*) 12 h with 10 μM FTY720-non-P

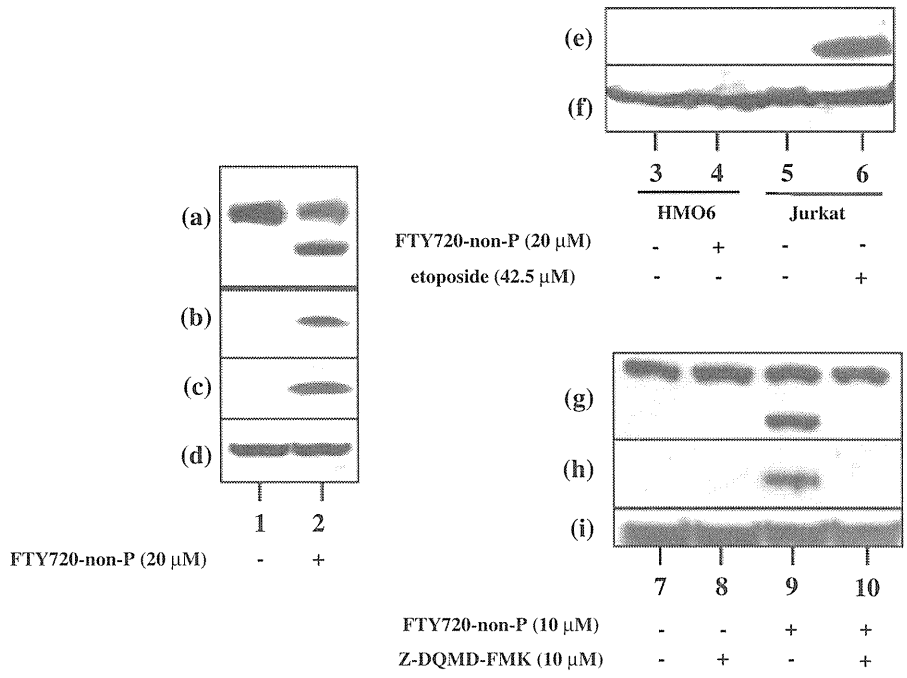

Fig. 3 FTY720-induced apoptosis of HMO6 was accompanied by activation of caspases 3 and 7. HMO6 cells were exposed for various time periods to varying concentrations of FTY720-non-P. For the positive control of caspase-9 activation, Jurkat cells were exposed to etoposide, an apoptosis-inducing agent. **a–i** indicate western blot of **a**, **g** PARP, **b** caspase-7 (a 20-kDa cleaved form), **c**, **h** caspase-3 (a 19-kDa cleaved form), **e** caspase-9 (a 37-kDa cleaved form), and **d**, **f**, **i** HSP60, an internal control of protein loading. The lanes (*1–10*) indicate HMO6 cells treated with (*1*, *3*) vehicle (DMSO) and (*2*, *4*) 20 μM FTY720-non-P for 9 h, and Jurkat cells treated with (*5*) vehicle (DMSO) and (*6*) 42.5 μM etoposide for 6 h, and (*7*) untreated HMO6 cells, and HMO6 cells treated with (*8*) 10 μM Z-DQMD-FMK, (*9*) 10 μM FTY720-non-P, and (*10*) a combination of 10 μM Z-DQMD-FMK and 10 μM FTY720-non-P for 12 h

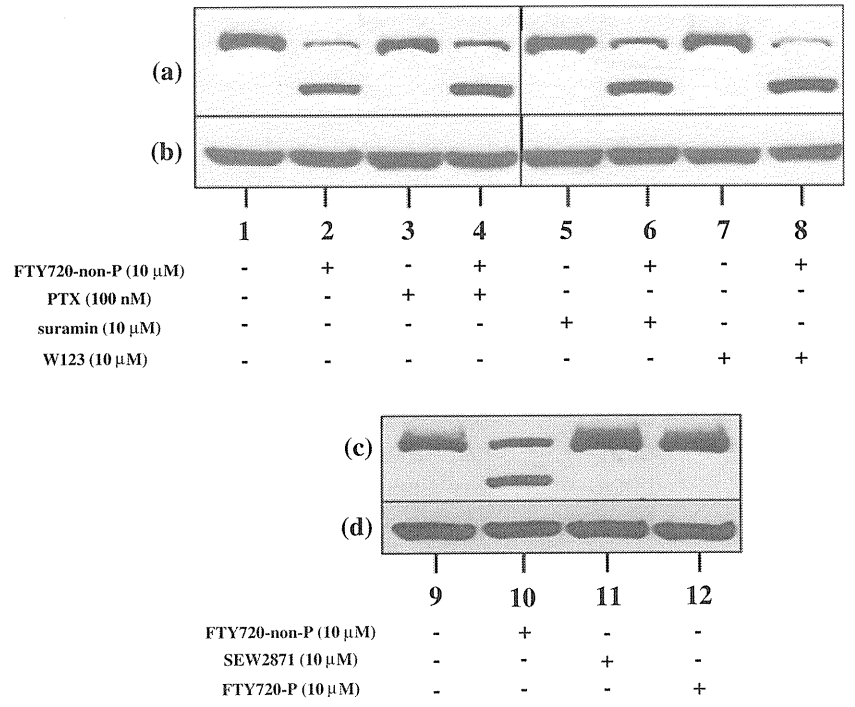

Fig. 4 FTY720-induced apoptosis of HMO6 was independent of S1P receptor binding. HMO6 cells were exposed for 12 h to 10 μM FTY720-non-P with or without inclusion of various S1P receptor agonists and antagonists. Pretreatment started at 30 min before exposure to FTY720-non-P. **a**–**d** indicate western blot of **a**, **c** PARP and **b**, **d** HSP60, an internal control of protein loading. The lanes (*1*–*12*) indicate (*1*, *9*) untreated HMO6 cells, and HMO6 cells treated with (*2*, *10*) 10 μM FTY720-non-P exposure alone, (*3*) 100 nM pertussis toxin (PTX) pretreatment alone, (4) 100 nM PTX pretreatment and 10 μM FTY720-non-P exposure, (*5*) 10 μM suramin pretreatment alone, (*6*) 10 μM suramin pretreatment and 10 μM FTY720-non-P exposure, (*7*) 10 μM W123 pretreatment alone, (*8*) 10 μM W123 pretreatment and 10 μM FTY720-non-P exposure, and HOM6 cells treated with a 12 h-exposure to (*11*) 10 μM SEW2871 or (*12*) 10 μM phosphorylated FTY720 (FTY720-P)

in HMO6 cells. The N-terminal fragment of SREBP2 is cleaved, dimerized, and translocated to the nucleus in response to the activating stimuli (Sato 2010). We identified the cleaved form of SREBP2 in HMO6 cells following an 1 h-exposure to FTY720-non-P ranging from 10 to 20 μM or by treatment with 3 μM simvastatin, a HMG-CoA reductase inhibitor capable of activating SREBP2 (Fig. 6a, lanes 2–4). Neither FTY720-non-P nor simvastatin alone at a concentration of 5 μM each induced apoptosis of HMO6 (Fig. 2a; Fig. 6b, lanes 7, 8). In contrast, a 12 h-pretreatment with 5 μM simvastatin enhanced FTY720-non-P-induced apoptosis of HMO6 cells, suggesting a proapoptotic effect mediated by SREBP2 activation following simvastatin treatment (Fig. 6b, lane 10).

A recent study showed that statins activate SREBP2, which positively controls the expression of caspase-7, resulting in induction of apoptosis of human gastric cancer cells (Gibot et al. 2009). When the N-terminal fragment of SREBP2 was overexpressed in HMO6 cells, the cleavage of PARP and caspase-3 was greatly enhanced, compared with the cells with overexpression of LacZ (Fig. 6c, f, lane 12), while the levels of procaspase-7 and cleaved caspase-7 were unaltered (Fig. 6g, lane 12).

Discussion

The present study revealed that non-phosphorylated FTY720 (FTY720-non-P) induced apoptosis of human microglia HM06 in a time- and dose-dependent manner with IC50 of 10.6 ± 2.0 μM. The apoptosis was inhibited by Z-DQMD-FMK, a caspase-3 inhibitor, but not by Pertussis toxin, a Gi protein inhibitor, suramin, a S1P3/S1P5 inhibitor, or W123, a S1P1 competitive antagonist, although HMO6 expressed S1P1, S1P2, and S1P3. Furthermore, both phosphorylated FTY720 (FTY720-P) and SEW2871, S1P1 selective agonists, did not induce apoptosis of HMO6. These observations suggest that FTY720-non-P-induced apoptosis of HMO6 cells is independent of S1P receptor binding.

Supporting these observations, FTY720, serving as a potential anti-cancer agent, induces apoptosis of various human cancer cell lines derived from liver, kidney, pancreas, and breast, multiple myeloma and leukemia cells, which is often mediated by S1P receptor-independent mechanisms (Matsuoka et al. 2003; Lee et al. 2004; Liu et al. 2010; Nagaoka et al. 2008). The concentrations required to induce apoptosis of tumor cells in vitro are about

Table 1 Upregulated genes in HMO6 following treatment with FTY720-non-P

Rank	Fold change	Entrez gene ID	Gene symbol	Gene name
1	5.75	25774	GSTTP1	Glutathione S-transferase theta pseudogene 1
2	3.16	150527	LOC150527	Hypothetical LOC150527
3	2.78	728380	RPL7P26	Ribosomal protein L7 pseudogene 26
4	2.74	3638	INSIG1	Insulin induced gene 1
5	2.72	158160	HSD17B7P2	Hydroxysteroid (17-beta) dehydrogenase 7 pseudogene 2
6	2.70	3157	HMGCS1	3-hydroxy-3-methylglutaryl-coenzyme A synthase 1 (soluble)
7	2.68	346007	EYS	Eyes shut homolog (Drosophila)
8	2.48	26834	RNU4-2	RNA, U4 small nuclear 2
9	2.46	163720	CYP4Z2P	Cytochrome P450, family 4, subfamily Z, polypeptide 2 pseudogene
10	2.44	54541	DDIT4	DNA-damage-inducible transcript 4
11	2.41	6351	CCL4	Chemokine (C–C motif) ligand 4
12	2.39	3949	LDLR	Low density lipoprotein receptor
13	2.37	6307	SC4MOL	Sterol-C4-methyl oxidase-like
14	2.34	286359	LOC286359	Hypothetical LOC286359
15	2.30	391003	PRAMEF18	PRAME family member 18
16	2.29	23175	LPIN1	Lipin 1
17	2.25	54897	CASZ1	Castor zinc finger 1
18	2.16	3156	HMGCR	3-hydroxy-3-methylglutaryl-coenzyme A reductase
19	2.16	196335	OR56B4	Olfactory receptor, family 56, subfamily B, member 4
20	2.10	3283	HSD3B1	Hydroxy-delta-5-steroid dehydrogenase, 3 beta- and steroid delta-isomerase 1
21	2.09	8553	BHLHE40	Basic helix-loop-helix family, member e40
22	2.07	10517	FBXW10	F-box and WD repeat domain containing 10
23	2.06	256892	OR51F1	Olfactory receptor, family 51, subfamily F, member 1
24	2.05	4598	MVK	Mevalonate kinase
25	2.04	196074	METT5D1	Methyltransferase 5 domain containing 1
26	2.04	901	CCNG2	Cyclin G2
27	2.03	439927	C1orf180	Chromosome 1 open reading frame 180
28	2.01	10551	AGR2	Anterior gradient homolog 2 (Xenopus laevis)
29	2.01	91074	ANKRD30A	Ankyrin repeat domain 30A
30	2.00	1831	TSC22D3	TSC22 domain family, member 3

HMO6 cells were exposed to non-phosporylated FTY720 (10 μM) or vehicle (DMSO) for 2 h. The genome-wide transcriptome was studied on Human Gene 1.0 ST array. The genes with an over 2-fold increase in FTY720-non-P-treated HMO6 cells are listed. The genes associated with steroid and/or sterol metabolism annotated by the DAVID program are underlined

two orders of magnitude greater than the blood concentration in the clinical setting, i.e., 5.4 ng/ml in plasma (Brinkmann et al. 2001, 2010). FTY720 has a half-life of approximately 10 days in vivo, and is cleared predominantly by a metabolic pathway requiring cytochrome P450 4F2 (CYP4F2) (Jin et al. 2011). The enzymatic activity of CYP4F2 is inhibited by certain drugs like ketoconazole, and the gene encoding CYP4F2 has a variety of single nucleotide polymorphisms (SNPs) (www.ncbi.nlm.nih.gov/snp). Therefore, in poor metabolizers of FTY720 receiving a CYP4F2 inhibitor, if they exist, the blood concentration of FTY720 could increase up to the range of toxic levels.

FTY720-non-P goes through the plasma membrane without requirement of the receptor binding, and targets directly key intracellular enzymes involved in sphingolipid metabolism, such as sphingosine kinases, phospholipase A2, and S1P lyase (Bandhuvula et al. 2005). FTY720 also inhibits ceramide synthases, resulting in a decrease in cellular levels of ceramide, dihydroceramide, shingosine, and S1P, and an increase in dihydrosphingosine and dihydroshingosine-1-phosphate, all of which alter the endogenous balance between survival and apoptotic signals (Berdyshev et al. 2009). FTY720-non-P promotes phosphorylation of 14-3-3zeta on Ser58 that disrupts 14-3-3 dimer formation, resulting in releasing proapototic mediators (Woodcock et al. 2010). FTY720, phosphorylated by SPHK2 located inside the plasma membrane, is transported outside the cells via the S1P transporter named spinster

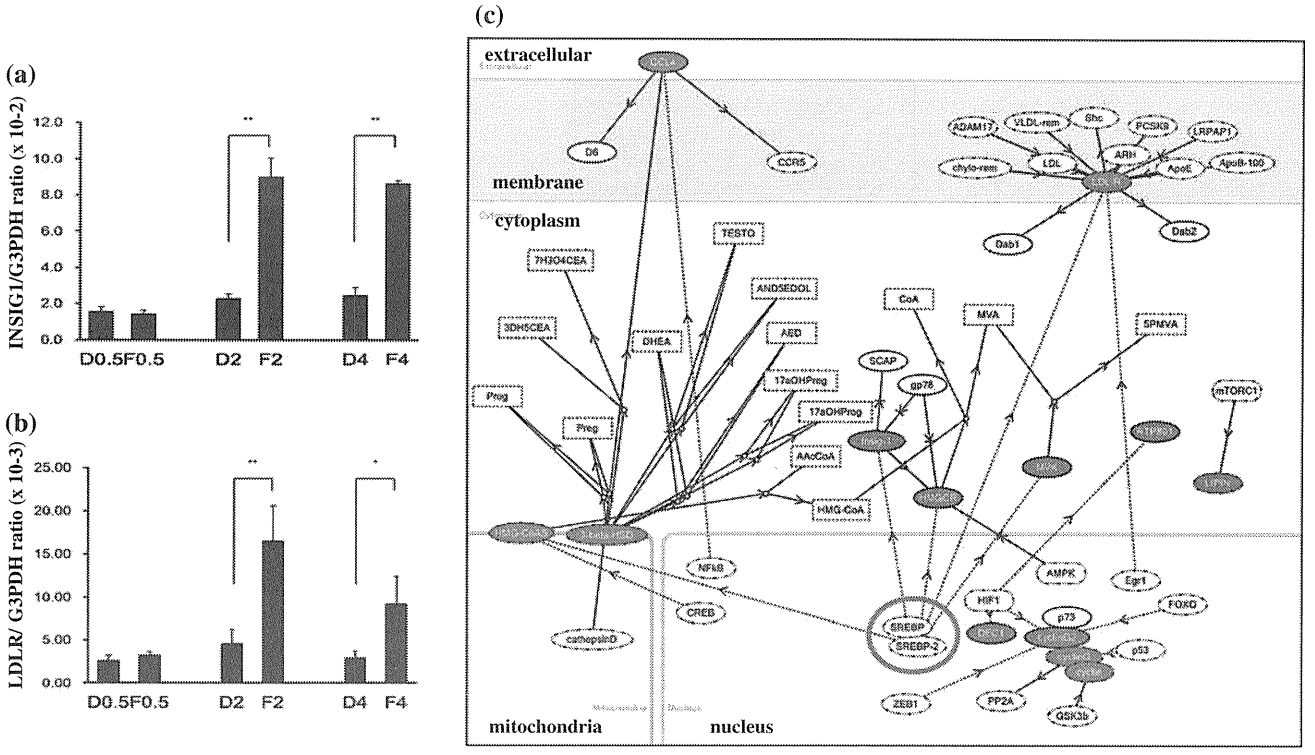

Fig. 5 FTY720 Induced SREBP-Responsive Genes. HMO6 cells were exposed for 2 h to 10 μM FTY720-non-P or vehicle (DMSO). Then, total RNA was processed for the genome-wide gene expression profiling on a microarray, followed by molecular network analysis by KeyMolnet and validation by qPCR. We identified 30 upregulated genes in FTY720-non-P-treated HMO6 cells (Table 1). **a**–**c** indicate qPCR of **a** INSIG1 and **b** LDLR, and **c** molecular network of FTY720-non-P-induced genes. Abbreviations: D, vehicle (DMSO); F, FTY720-non-P; 0.5, 30 min; 2, 2 h; and 4, 4 h. In **c**, red filled nodes represent FTY720-non-P-induced genes, whereas white open nodes exhibit additional nodes extracted automatically from the core contents of KeyMolnet to establish molecular connections. The molecular relation is indicated by solid line with arrow (direct binding or activation), solid line with arrow and stop (direct inactivation), solid line without arrow (complex formation), dash line with arrow (transcriptional activation), and dash line with arrow and stop (transcriptional repression). The transcription factor SREBP (SREBP2) is highlighted by a red thick circle

homolog 2 (SPNS2), and then the phosphorylated FTY720 binds to S1P receptors expressed on the surface of the plasma membrane (Hisano et al. 2011).

Being consistent with our observations, FTY720-non-P but not FTY720-P induces apoptosis of human breast and colon cancers (Nagaoka et al. 2008). FTY720 inhibits cytosolic phospholipase A2 ($cPLA_2$) in a manner independent of S1P receptor binding (Payne et al. 2007). FTY720-non-P but not FTY720-P inhibits PKC activation, which is associated with cell-surface expression of S1P1 (Sensken and Gräler 2010). Furthermore, FTY720-P counteracts FTY720-non-P-induced apoptosis of human fibroblasts by activating Bcl-2 (Potteck et al. 2010).

Several previous studies showed that FTY720-induced apoptosis is often accompanied by activation of a series of caspases (Wang et al. 1999). We found activation of both caspase-3 and caspase-7 during FTY720-non-P-induced apoptosis of HMO6. Furthermore, FTY720-induced apoptosis also involves various mechanisms, such as dephosphorylation of protein kinase B (Akt) (Matsuoka et al. 2003; Lee et al. 2004), deregulation of mitogen-activated protein kinases (MAPKs), focal adhesion kinase (FAK), and Rho-GTPase (Matsuda et al. 1999; Sonoda et al. 2001), and activation of protein phosphatase 2A (PP2A) (Liu et al. 2010). Here, we for the first time showed that FTY720-non-P-induced apoptosis of HMO6 cells is positively regulated by the SREBP2-dependent signaling pathway.

A recent study showed that statins induce apoptosis of human gastric cancer cells by activating SREBP1 and SREBP2, both of which transcriptionally upregulate caspase-7 (Gibot et al. 2009). Statin-dependent apoptosis is prevented by replenishment of mevalonate, the immediate product by the HMG-CoA reductase activity (Xia et al. 2001). A previous study showed that activation of caspase-3 releases SREBP proteins from ER membrane in a proteolytic reaction distinct from the sterol-regulated cleavage, resulting in nuclear transport of SREBP and transcriptional activation of sterol-regulatory genes (Higgins and Ioannou 2001). However, during FTY720-non-P-induced apoptosis of HMO6 cells, we identified activation of SREBP2 as early as at 1 h after initiation of the treatment, which is long before detection of the PARP cleavage, suggesting that

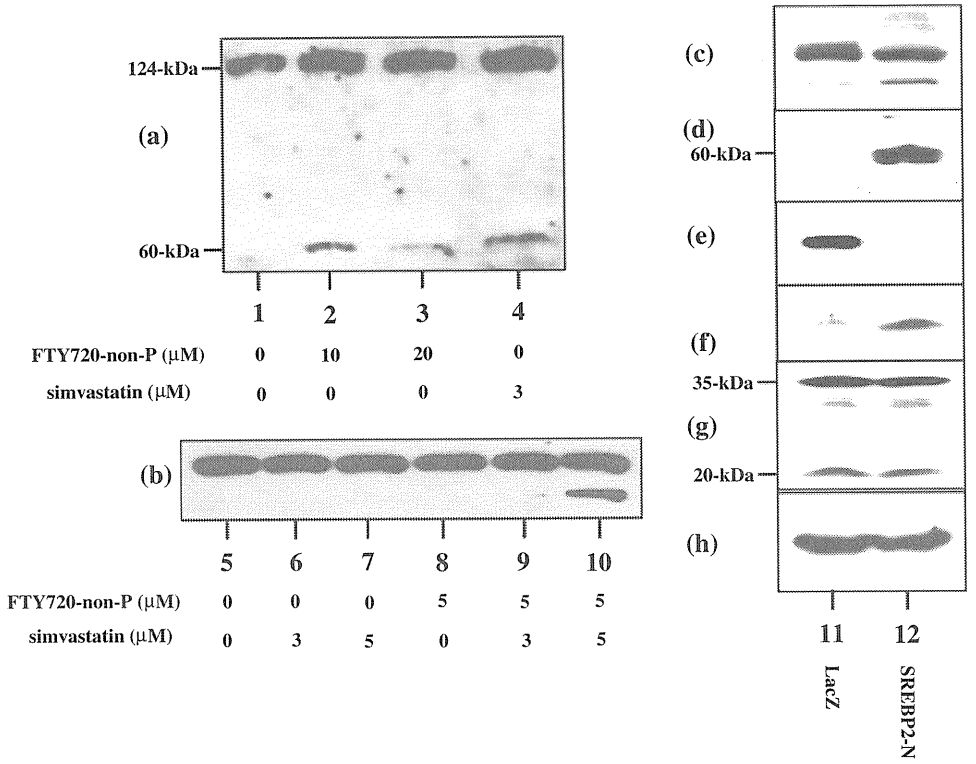

Fig. 6 Activation of SREBP2 by FTY720-non-P in HMO6 cells. HMO6 cells were exposed to FTY720-non-P or simvastatin, or transfected with the vector expressing the N-terminal fragment of SREBP2 (SREBP2-N) or LacZ. **a–h** indicate western blot of **a**, **d** SREBP2, **b**, **c** PARP, **e** V5, **f** cleaved caspase-3, **g** caspase-7 (a 35-kDa proform and a 20-kDa cleaved form), and **h** HSP60. The lanes *1–12* represent (*1*, *5*) untreated HMO6 cells, and HMO6 cells treated for 1 h with (*2*) 10 μM FTY720-non-P, (*3*) 20 μM FTY720-non-P, (*4*) 3 μM simvastatin, and HMO6 cells pretreated for simvastatin starting at 12 h before a 6 h-exposure to FTY720-non-P, whose conditions are composed of (*6*) 3 μM simvastatin pretreatment alone, (*7*) 5 μM simvastatin pretreatment alone, (*8*) no simvastatin pretreatment and 5 μM FTY720-non-P exposure, (*9*) 3 μM simvastatin pretreatment and 5 μM FTY720-non-P exposure, and (*10*) 5 μM simvastatin pretreatment and 5 μM FTY720-non-P exposure, and HMO6 cells with overexpression of (*11*) V5-tagged LacZ or (*12*) SREBP2-N

SREBP activation is not a secondary phenomenon following caspase-3 activation. Furthermore, we found that activation of SREBP2 by overexpression of the N-terminal fragment of SREBP2 in HMO6 cells enhances the cleavage of PARP and caspase-3 in the absence of FTY720. Moreover, we found that pretreatment with simvastatin enhanced FTY720-non-P-induced apoptosis of HMO6 cells. Statins activate SREBP2 and induce apoptosis of various cells (Xia et al. 2001; Gibot et al. 2009). All of these observations suggest that the SREBP2-dependent signaling pathway is intrinsically proapoptotic, when it is aberrantly regulated.

A recent study showed that FTY720 inhibits intracellular transport of cholesterol to ER in human macrophages, being independent of S1P1 binding, indicating that FTY720-non-P certainly affects the cellular cholesterol processing (Blom et al. 2010). Importantly, cholesterol interacts specifically with sphingosine in human intestinal epithelial cells under physiological conditions (Garmy et al. 2005). S1P is intracellularly generated by sphingosine kinases SPHK1 and SPHK2 from sphingosine, a breakdown product of the cell membrane constituent sphingomyelin (Chi 2011). S1P and its synthetic analog FTY720-P share S1P1, S1P3, S1P4, and S1P5 expressed on the plasma membrane. All of these observations propose a possible scenario that excessive amounts of intracellular FTY720-non-P disturb the complex metabolic network of cholesterols and sphingolipids, resulting in activation of the SREBP2-dependent proapoptotic signaling pathway.

Acknowledgments This work was supported by grants from the Research on Intractable Diseases, the Ministry of Health, Labour and Welfare, Japan (H22-Nanchi-Ippan-136; H21-Nanchi-Ippan-201; H21-Nanchi Ippan-217; H21-Kokoro-Ippan-018) and the High-Tech Research Center Project (S0801043) and the Grant-in-Aid (C22500322), the Ministry of Education, Culture, Sports, Science and Technology (MEXT), Japan. The microarray data are available from Gene Expression Omnibus (GEO) under the accession number GSE28642.

References

Bandhuvula P, Tam YY, Oskouian B, Saba JD (2005) The immune modulator FTY720 inhibits sphingosine-1-phosphate lyase activity. J Biol Chem 280:33697–33700

Berdyshev EV, Gorshkova I, Skobeleva A, Bittman R, Lu X, Dudek SM, Mirzapoiazova T, Garcia JG, Natarajan V (2009) FTY720 inhibits ceramide synthases and up-regulates dihydrosphingosine 1-phosphate formation in human lung endothelial cells. J Biol Chem 284:5467–5477

Blom T, Bäck N, Mutka AL, Bittman R, Li Z, de Lera A, Kovanen PT, Diczfalusy U, Ikonen E (2010) FTY720 stimulates 27-hydroxycholesterol production and confers atheroprotective effects in human primary macrophages. Circ Res 106:720–729

Brinkmann V, Wilt C, Kristofic C, Nikolova Z, Hof RP, Chen S, Albert R, Cottens S (2001) FTY720: dissection of membrane receptor-operated, stereospecific effects on cell migration from receptor-independent antiproliferative and apoptotic effects. Transplant Proc 33:3078–3080

Brinkmann V, Billich A, Baumruker T, Heining P, Schmouder R, Francis G, Aradhye S, Burtin P (2010) Fingolimod (FTY720): discovery and development of an oral drug to treat multiple sclerosis. Nat Rev Drug Discov 9:883–897

Chi H (2011) Sphingosine-1-phosphate and immune regulation: trafficking and beyond. Trends Pharmacol Sci 32:16–24

Choi JW, Gardell SE, Herr DR, Rivera R, Lee CW, Noguchi K, Teo ST, Yung YC, Lu M, Kennedy G, Chun J (2011) FTY720 (fingolimod) efficacy in an animal model of multiple sclerosis requires astrocyte sphingosine 1-phosphate receptor 1 (S1P1) modulation. Proc Natl Acad Sci USA 108:751–756

Coelho RP, Payne SG, Bittman R, Spiegel S, Sato-Bigbee C (2007) The immunomodulator FTY720 has a direct cytoprotective effect in oligodendrocyte progenitors. J Pharmacol Exp Ther 323:626–635

da Huang W, Sherman BT, Lempicki RA (2009) Systematic and integrative analysis of large gene lists using DAVID bioinformatics resources. Nat Protoc 4:44–57

Dev KK, Mullershausen F, Mattes H, Kuhn RR, Bilbe G, Hoyer D, Mir A (2008) Brain sphingosine-1-phosphate receptors: implication for FTY720 in the treatment of multiple sclerosis. Pharmacol Ther 117:77–93

Durafourt BA, Lambert C, Johnson TA, Blain M, Bar-Or A, Antel JP (2011) Differential responses of human microglia and blood-derived myeloid cells to FTY720. J Neuroimmunol 230:10–16

Garmy N, Taïeb N, Yahi N, Fantini J (2005) Interaction of cholesterol with sphingosine: physicochemical characterization and impact on intestinal absorption. J Lipid Res 46:36–45

Gibot L, Follet J, Metges JP, Auvray P, Simon B, Corcos L, Le Jossic-Corcos C (2009) Human caspase 7 is positively controlled by SREBP-1 and SREBP-2. Biochem J 420:473–483

Higgins ME, Ioannou YA (2001) Apoptosis-induced release of mature sterol regulatory element-binding proteins activates sterol-responsive genes. J Lipid Res 42:1939–1946

Hisano Y, Kobayashi N, Kawahara A, Yamaguchi A, Nishi T (2011) The sphingosine 1-phosphate transporter, SPNS2, functions as a transporter of the phosphorylated form of the immunomodulating agent FTY720. J Biol Chem 286:1758–1766

Jack C, Ruffini F, Bar-Or A, Antel JP (2005) Microglia and multiple sclerosis. J Neurosci Res 81:363–373

Jin Y, Zollinger M, Borell H, Zimmerlin A, Patten CJ (2011) CYP4F enzymes are responsible for the elimination of fingolimod (FTY720), a novel treatment of relapsing multiple sclerosis. Drug Metab Dispos 39:191–198

Kappos L, Antel J, Comi G, Montalban X, O'Connor P, Polman CH, Haas T, Korn AA, Karlsson G, Radue EW, FTY720 D2201 Study Group (2006) Oral fingolimod (FTY720) for relapsing multiple sclerosis. N Engl J Med 355:1124–1140

Lee TK, Man K, Ho JW, Sun CK, Ng KT, Wang XH, Wong YC, Ng IO, Xu R, Fan ST (2004) FTY720 induces apoptosis of human hepatoma cell lines through PI3-K-mediated Akt dephosphorylation. Carcinogenesis 25:2397–2405

Liu Q, Alinari L, Chen CS, Yan F, Dalton JT, Lapalombella R, Zhang X, Mani R, Lin T, Byrd JC, Baiocchi RA, Muthusamy N (2010) FTY720 shows promising in vitro and in vivo preclinical activity by downmodulating cyclin D1 and phospho-Akt in mantle cell lymphoma. Clin Cancer Res 16:3182–3192

Matsuda S, Minowa A, Suzuki S, Koyasu S (1999) Differential activation of c-Jun NH2-terminal kinase and p38 pathways during FTY720-induced apoptosis of T lymphocytes that is suppressed by the extracellular signal-regulated kinase pathway. J Immunol 162:3321–3326

Matsuoka Y, Nagahara Y, Ikekita M, Shinomiya T (2003) A novel immunosuppressive agent FTY720 induced Akt dephosphorylation in leukemia cells. Br J Pharmacol 138:1303–1312

Miron VE, Jung CG, Kim HJ, Kennedy TE, Soliven B, Antel JP (2008) FTY720 modulates human oligodendrocyte progenitor process extension and survival. Ann Neurol 63:61–71

Miron VE, Ludwin SK, Darlington PJ, Jarjour AA, Soliven B, Kennedy TE, Antel JP (2010) Fingolimod (FTY720) enhances remyelination following demyelination of organotypic cerebellar slices. Am J Pathol 176:2682–2694

Mullershausen F, Zecri F, Cetin C, Billich A, Guerini D, Seuwen K (2009) Persistent signaling induced by FTY720-phosphate is mediated by internalized S1P1 receptors. Nat Chem Biol 5: 428–434

Nagai A, Nakagawa E, Hatori K, Choi HB, McLarnon JG, Lee MA, Kim SU (2001) Generation and characterization of immortalized human microglial cell lines: expression of cytokines and chemokines. Neurobiol Dis 8:1057–1068

Nagaoka Y, Otsuki K, Fujita T, Uesato S (2008) Effects of phosphorylation of immunomodulatory agent FTY720 (fingolimod) on antiproliferative activity against breast and colon cancer cells. Biol Pharm Bull 31:1177–1181

Narantuya D, Nagai A, Sheikh AM, Masuda J, Kobayashi S, Yamaguchi S, Kim SU (2010) Human microglia transplanted in rat focal ischemia brain induce neuroprotection and behavioral improvement. PLoS One 5:e11746

Payne SG, Oskeritzian CA, Griffiths R, Subramanian P, Barbour SE, Chalfant CE, Milstien S, Spiegel S (2007) The immunosuppressant drug FTY720 inhibits cytosolic phospholipase A2 independently of sphingosine-1-phosphate receptors. Blood 109: 1077–1085

Potteck H, Nieuwenhuis B, Lüth A, van der Giet M, Kleuser B (2010) Phosphorylation of the immunomodulator FTY720 inhibits programmed cell death of fibroblasts via the S1P3 receptor subtype and Bcl-2 activation. Cell Physiol Biochem 26:67–78

Sato R (2010) Sterol metabolism and SREBP activation. Arch Biochem Biophys 501:177–181

Satoh J, Tabunoki H, Arima K (2009) Molecular network analysis suggests aberrant CREB-mediated gene regulation in the Alzheimer disease hippocampus. Dis Markers 27:239–252

Sensken SC, Gräler MH (2010) Down-regulation of S1P1 receptor surface expression by protein kinase C inhibition. J Biol Chem 285:6298–6307

Sonoda Y, Yamamoto D, Sakurai S, Hasegawa M, Aizu-Yokota E, Momoi T, Kasahara T (2001) FTY720, a novel immunosuppressive agent, induces apoptosis in human glioma cells. Biochem Biophys Res Commun 281:282–288

Van Doorn R, Van Horssen J, Verzijl D, Witte M, Ronken E, Van Het Hof B, Lakeman K, Dijkstra CD, Van Der Valk P, Reijerkerk A, Alewijnse AE, Peters SL, De Vries HE (2010) Sphingosine 1-phosphate receptor 1 and 3 are upregulated in multiple sclerosis lesions. Glia 58:1465–1476

Wang JD, Takahara S, Nonomura N, Ichimaru N, Toki K, Azuma H, Matsumiya K, Okuyama A, Suzuki S (1999) Early induction of apoptosis in androgen-independent prostate cancer cell line by FTY720 requires caspase-3 activation. Prostate 40:50–55

Wei Y, Yemisci M, Kim HH, Yung LM, Shin HK, Hwang SK, Guo S, Qin T, Alsharif N, Brinkmann V, Liao JK, Lo EH, Waeber C (2011) Fingolimod provides long-term protection in rodent models of cerebral ischemia. Ann Neurol 69:119–129

Woodcock JM, Ma Y, Coolen C, Pham D, Jones C, Lopez AF, Pitson SM (2010) Sphingosine and FTY720 directly bind pro-survival 14-3-3 proteins to regulate their function. Cell Signal 22: 1291–1299

Xia Z, Tan MM, Wong WW, Dimitroulakos J, Minden MD, Penn LZ (2001) Blocking protein geranylgeranylation is essential for lovastatin-induced apoptosis of human acute myeloid leukemia cells. Leukemia 15:1398–1407

Zhang Z, Zhang Z, Fauser U, Artelt M, Burnet M, Schluesener HJ (2007) FTY720 attenuates accumulation of EMAP-II+ and MHC-II+ monocytes in early lesions of rat traumatic brain injury. J Cell Mol Med 11:307–314

RESEARCH ARTICLE

International Journal of Geriatric Psychiatry

Relationship between white matter T2 hyperintensity and cortical volume changes on magnetic resonance imaging in healthy elders

Miho Ota[1,2], Kiyotaka Nemoto[2], Noriko Sato[1], Katsutoshi Mizukami[3], Fumio Yamashita[4] and Takashi Asada[3]

[1]Department of Radiology, National Center of Neurology and Psychiatry, Ogawahigashi, Kodaira, Tokyo, Japan
[2]Division of Psychiatry, Tsukuba University Hospital, Amakubo, Tsukuba, Ibaraki, Japan
[3]Departments of Neuropsychiatry, Institute of Clinical Medicine, University of Tsukuba, Tennoudai, Tsukuba, Ibaraki, Japan
[4]Department of Psychiatry, Institute of Clinical Medicine, University of Tsukuba, Tennoudai, Tsukuba, Ibaraki, Japan
Correspondence to: M. Ota, E-mail: ota@ncnp.go.jp

Objective: T2 white matter hyperintensity (WMH) on magnetic resonance imaging (MRI) is associated with brain atrophy. Some previous studies examined the relation between the WMH and cortical atrophy, however, little is known about how the WMHs affect the pattern of cortical atrophy. Recent studies have revealed that patho-physiological role of WMH in affecting cortical atrophy may be different between hyperintensities in basal ganglia and thalami (B&T) and those in other regions. Based on a longitudinal study up to 5 years, we attempt to examine the temporal relation between the WMHs and cortical atrophy with special attention to the hyperintensities in the B&T.

Methods: We evaluated the temporal pattern of cortical atrophy in 74 cognitively normal subjects lacking hyperintensities in B&T (first analysis) and 13 cognitively normal subjects with hyperintensities in B&T (second analysis). The relationship between the baseline WMH severity and the cortical volume change during the observation period (mean: 3.8 years) was voxel basically evaluated on the images.

Results: The first analysis showed fairly axisymmetrical atrophy pattern in parietal, occipital, and precentral cortices, while the findings gained from the second appear to lack such systematic orderliness of the atrophy.

Conclusion: This result shows that WMH may affect atrophy in multiple cerebral cortices even in cognitively normal subjects. Understanding the impact of WMH on the shrinkage shown in the brains of cognitively healthy older individuals is an important base for assessing the temporal pattern of atrophy of the individual with neurodegenerative disorder like AD. Copyright © 2010 John Wiley & Sons, Ltd.

Key words: white matter hyperintensity; magnetic resonance imaging; older
History: Received 15 June 2010; Accepted 21 July 2010; Published online 24 September 2010 in Wiley Online Library (wileyonlinelibrary.com).
DOI: 10.1002/gps.2618

Introduction

White matter hyper-intensities (WMH) defined as areas with high signal intensities on T2-weighted magnetic resonance imaging (MRI) are commonly found on MRI of older individuals. They have been reported to be related with cognitive impairment and vascular pathology even in the healthy older. The WMH affect cognitive function including the speed of cognitive processes and executive function (Junqué *et al.*, 1990; Schmidt *et al.*, 1993), which is presumably associated with brain atrophy and reduced cerebral blood flow (Mirsen *et al.*, 1991; De Reuck *et al.*, 1992; Du *et al.*, 2005; Mungas *et al.*, 2005; Wen *et al.*, 2006). Pathology of WMH may be attributable to dilatation of periventricular space, peri-vascular demyelination, and gliosis. Several researchers have examined the patho-physiological role of WMH in affecting cortical atrophy of the healthy and pathological brains of the older.

Recently, mild cognitive impairment (MCI) which is a distinct state of abnormal cognition that does not amount to dementia but is distinguishable from

normal cognitive decline associated with aging has attracted an increasing attention, because it may offer opportunities for very early diagnosis of Alzheimer's disease (AD). One study reported that high WMH prevalence strongly predicted the progression from normal to MCI (Smith *et al.*, 2008).

Another study showed difference in the level of WMH between the MCI to AD converter and non-converters (Misra *et al.*, 2009). Although whether the patho-physiology of AD is directly associated with vascular pathological changes remain an open question, it appears that the clinical manifestation of AD is highly correlated with the vascular pathology (Misra *et al.*, 2009). AD patients are likely to have more extensive WMH than age-matched controls (Scheltens *et al.*, 1992).

Taking such information into consideration, it is very important to examine the pattern and mechanism of WMH on cortical atrophy among cognitively healthy individuals is very important for the basis of the assessment for the pattern and mechanism among individuals with pathological conditions including AD.

Most of the previous studies regarding the association between WMH and the cortical atrophy examined the correlation between the load for whole brain WMHs and shrinkage of whole brain gray matter (Mirsen *et al.*, 1991; Du *et al.*, 2005; Mungas *et al.*, 2005), thus little is known about the effect of WMH on the regional cortical atrophy. An exceptional study reported that the WMHs in the frontal lobe were correlated with the change in the volume of frontal cortex (Tullberg *et al.*, 2004). Another study also showed that subjects with WHM loads located mainly in frontal lobe showed bilateral frontal cortical atrophy (Rossi *et al.*, 2006). Furthermore, a study showed the correlation between the cortical change of each lobe and WMHs in its corresponding white matter (Wen *et al.*, 2006). It is of note that all of these studies are cross-sectional design, and no previous study has examined the relation longitudinally.

Recent development of the diffusion tensor imaging technique enabled the depiction of projecting neural fibers non-invasively (Behrens *et al.*, 2003). The development has revealed that basal ganglia and thalami (B&T) mediate communication over widespread areas of the cortex with neural fibers as the central relay station in the brain. The hyperintensity in T2-weighted images of B&T may affect not only volume change of themselves but also the cerebral cortex to which B&T connect. In addition, some researchers have reported that the disturbance of cerebral cortex conversely affects the volume change of basal ganglia (Ogawa *et al.*, 1997; Ota *et al.*, 2007). Therefore, for the accurate estimation of the influence of the WMH on cortical volume loss, it may be appropriate that hyperintensity on T2-weighted images in B&T and that in other regions should be dealt separately. However, previous quantitative studies, automatically calculated the volume of WMHs of the whole brain, thus they did not distinguish hyperintensities on T2-weighted image in B&T from those in other regions. Some studies evaluated the relationship between the regional cortical volume and the WMH loads voxel based on a lobe-to-lobe basis (Rossi *et al.*, 2006; Wen *et al.*, 2006). However, it is known that WMHs in any brain region cause other cortical changes (Tullberg *et al.*, 2004; Rossi *et al.*, 2006; Wen *et al.*, 2006). Additionally, because too many factors are involved in the interaction, it is difficult to evaluate the relationship between the atrophy and the WMHs.

In this study, we have conducted a follow-up brain MRI study for the older individuals participating in a community-based study. In order to easily exclude the subjects with hyperintensities in B&T, we adopted qualitative morphometry based on the grading of local WMHs and identified the subjects without hyperintensities on T2-weighted image in B&T. We examined the correlation between the severity of baseline-scan WMH for whole brain and the atrophy rate of the regional cortex using voxel-based morphometry.

Methods

This study was conducted as a part of a community-based project aiming at prevention of dementia in the older. The details of the project have been reported elsewhere, so the description of the method here will be given in brief (Miyamoto *et al.*, 2009). The protocol for this study was approved by the ethics committee of the University of Tsukuba and all participants gave their informed consent.

At the baseline, between December 2001 and April 2002, 1888 out of the 2698 candidate inhabitants who were 65 years or older underwent the cognitive assessment using a battery of neuropsychological tests (Sasaki *et al.*, 2009); category-cued recall (Grober *et al.*, 1998); set-dependency activity (Sohlberg and Mateer, 1986); category verbal fluency (Monsch *et al.*, 1992); clock-drawing test (Brodaty and Moore, 1997); and Wechsler Adult Intelligence Scale Revised (WAIS-R) (Wechsler, 1981). We regarded the subject who marked score less than 1 SD below the demographically corrected mean on each of the five cognitive domains to fall short of normal limits (Miyamoto *et al.*, 2009).

According to our invitation, 284 self-selected subjects underwent brain MRI scanning. A total of 172 individuals out of the 284 were diagnosed as having normal cognitive function and no abnormal MRI findings such as cortical infarctions, brain tumors, or head injury. We defined infarct as high intensity lesion having a size of ≧3 mm on T2-weighted images and low intensity on T1-weighted images, following the criteria of the Workshop Study (Adachi *et al.*, 2002). They were selected as the participants for the present longitudinal MRI study. Using Fazekas criterion for the severity of WMH, we defined Fazekas 2 or 3 as severe hyperintensity (Wahlund *et al.*, 2001).

Eighty-seven out of the 172 participants were cognitively healthy both at the baseline and the end of the observation period, and underwent annual MRI scanning at least four times. From these 87 participants, we excluded 13 subjects with severe hyperintensity located in B&T on the images of the baseline-scan. For the first analysis, the data from cognitively healthy 74 subjects (39 men, 35 women; mean age, 72.3 ± 3.8 years; mean years of education, 10.9 ± 3.1 years; mean mini-mental state examination (MMSE) score, 28.4 ± 1.8 at the baseline, scan interval = 3.8 ± 0.2) lacking hyperintensities in B&T were used. For the second analysis, the 13 subjects with severe hyperintensities in B&T (4 men, 9 women; mean age, 75.4 ± 4.4 years; mean years of education, 10.4 ± 3.2 years; mean MMSE score, 27.8 ± 2.4 at the baseline, scan interval = 3.8 ± 0.1) were employed.

The clinical characteristics of the subjects are presented in Table 1. We used a pair of MRI data with for each participant.

First, cranial MRI was performed using a 1.5-T Magnetom Symphony system (Siemens, Erlangen, Germany). Conventional axial T2-weighted turbo spin echo images were obtained using the following settings: repetition time (TR), 4000 ms; echo time (TE), 96 ms; slice thickness, 5 mm; intersection gap, 1.5 mm; matrix, 512 × 512; field of view, 230 × 230 mm; number of signals acquired, 2. In addition to T2-weighted imaging, high spatial-resolution, 3-dimensional (3D) T1-weighted imaging was also used for the study. Scans for 3D T1-weighted imaging were made in the sagittal plane using the following settings: TR, 2080 ms; TE, 3.93 ms; flip angle, 12°; effective section thickness, 1.20 mm; slab thickness, 173 mm; matrix, 512 × 512; field of view, 280 × 280 mm; number of signals acquired, 1. This yielded 144 contiguous slices through the head.

To clarify the relationship between the rate of cortical gray matter volume change and the severity of WMH, structural 3D T1-weighted MR images were analyzed using an optimized voxel-based morphometry (VBM) technique. Data were computed using Statistical Parametric Mapping 5 (SPM5) software (Wellcome Department of Imaging Neuroscience, London, UK) running on MATLAB 7.0 (Math Works, Natick, MA). Optimized VBM were processed using SPM5 tool software. Details of this process are described elsewhere (Good *et al.*, 2001). Normalized segmented images were modulated by multiplication with Jacobian determinants of spatial normalization function to encode the deformation field for each subject as tissue density changes in normal space. The atrophy rate of the regional gray matter was computed by comparing the modulated segmented scan image

Table 1 Descriptive characteristics of the study sample without white matter hyperintensities in basal ganglia and thalami (Fazekas <2; (a), $N = 74$) and with hyperintensities in basal ganglia and thalami (Fazekas ≧2; (b), $N = 13$)

The degree of subcortical white matter changes	Age (year) (quartile; median)	Sex	MRI period (year) (quartile; median)	Education (year) (quartile; median)	MMSE (quartile; median)
(a)					
Fazekas = 0	69–73	M: 23; F: 24	3.6–3.8	8–12	27–30
	71		3.7	11	29
Fazekas = 1	69.8–74.5	M: 11; F: 5	3.7–3.8	11–12	27–30
	72		3.7	12	29
Fazekas = 2	75–78	M: 4; F: 5	3.7–3.8	8–12	28–30
	77		3.7	8	30
Fazekas = 3	76–78 (range)	M: 1; F: 1	3.6–3.8 (range)	11–11 (range)	27–30 (range)
(b)					
Fazekas = 0		M: 0; F: 0			
Fazekas = 1	72.5–75.8	M: 1; F: 3	3.8–4.0	8.3–11.5	28.8–30
	74		3.9	9.5	29.5
Fazekas = 2	73.5–78	M: 2; F: 5	3.7–3.8	8–17	25–29.5
	76		3.8	12.5	26
Fazekas = 3	74–76 (range)	M: 1; F: 1	3.8–3.9 (range)	8–17 (range)	25–30 (range)

at the baseline (I_b) and at the follow up (I_f) (Fotenos *et al.*, 2005).

$$\text{Atrophy rate} = \frac{(I_b - I_f)}{I_b}$$

Images of the atrophy rate were smoothed using a 8 mm full-width half-maximum of an isotropic Gaussian kernel.

For the present analysis, we took the severity of WMH into consideration. The levels for overall severity of white matter excluding B&T were divided into four: 0, no lesion; 1, focal lesions in at least one lobe; 2, beginning confluence of lesions in at least one lobe; 3, diffuse lesions in all over white mattes (Figure 1), and 0, no lesion; 1, focal lesions; 2, >1 focal lesions, and 3, confluent lesions for B&T (DeCarli *et al.*, 2005).

Two trained operators rated the overall severity for white matter excluding B&T and the severity of B&T of the 84 participants, and the reproducibility was calculated. The intra-class correlation coefficients (ICCs) for these measurements were 0.85 and 0.95, respectively. ICC values over 0.75 indicate good reliability, so our rating is considered to be reliable (Landis and Koch, 1977).

The relationship between the atrophy rate of regional gray matter volume and the severity of WMH at the baseline scan was evaluated using a single regression model. Only correlations that had a cluster level of $p < 0.001$ (uncorrected) with an extent threshold criterion of more than 300 contiguous voxels were considered statistically to be significant. For the evaluation of the effect of WMH on the gray matter volume, the result was masked with the gray matter image derived from the WFU_pickatlas (Maldjian *et al.*, 2003). Subsequently, we evaluated the correlation between severity of the WMH and progression of the brain atrophy using age as a nuisance variable. We regarded the criteria same as above (a cluster level of $p < 0.001$ (uncorrected) with an extent threshold criterion of more than 300 contiguous voxels) as statistically significant, too. Only this process, statistical analysis was performed using SPM2.

We also evaluated the differences among the four levels (Fazekas = 0, 1, 2, and 3) according to age, sex, MMSE score, years of education, and scan interval using one-way ANOVA. Statistical analyses were performed using SPSS for Windows 11.0.1J software (SPSS Japan, Tokyo, Japan).

Results

The first analysis for the 74 subjects lacking hyperintensities in B&T showed significant positive correlations between the atrophy rate of regional gray matter and severity of WMH in the bilateral parietal and occipital cortices axisymmetrically, birateral precentral gyri, and right frontal cortex (Figure 2). The analyses showed no significant difference in sex, MMSE score, years of education, and scan interval among the four groups. However, only a significant difference in age

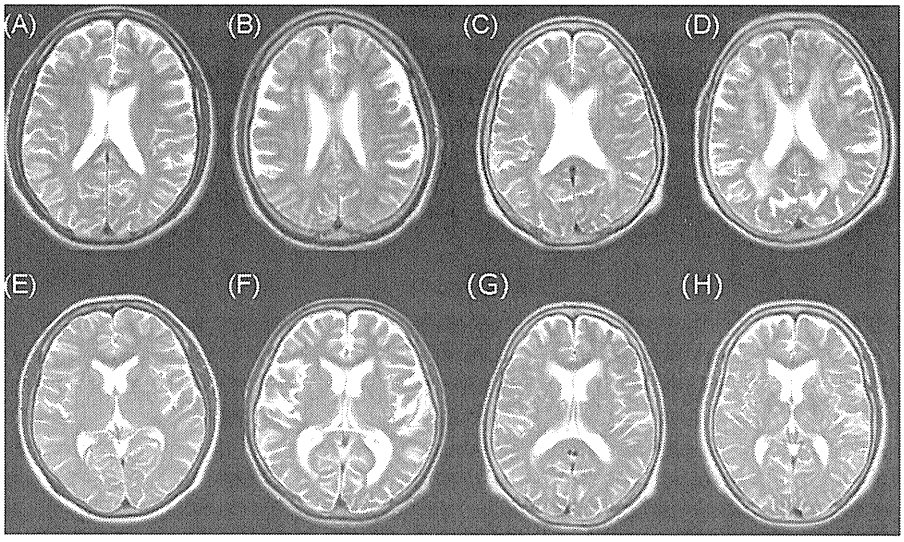

Figure 1 (A–H) Examples of rating scores 0, 1, 2, and 3 on cerebral T2-weighted imaging. Upper column: definitions of rating scores for white matter lesions: 0, no lesion (A); 1, focal lesions (B); 2, beginning confluence of lesions (C); 3, diffuse lesions in all over white mattes (D). Lower column: definitions of rating scores for basal ganglia and thalami: 0, no lesion (E); 1, focal lesions (F); 2, >1 focal lesions (G), and 3, confluent lesions (H).

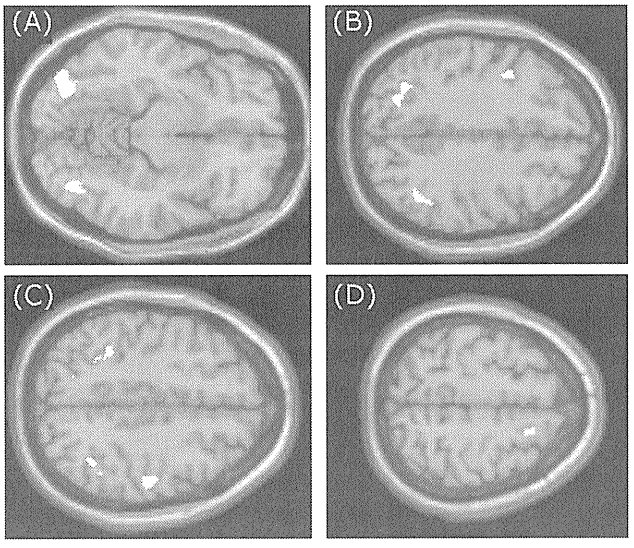

Figure 2 The relationship between the atrophy rate of regional gray matter volume and WMH severity at the baseline scan was evaluated in 74 participants without the hyperintensity in basal ganglia (single regression model, SPM5). There were positive correlations between WMH severity and the atrophy rate of the regional gray matter volume of (A) the bilateral occipital corti, (B) the bilateral parietal corti and left precentral gyrus, (C) the right precentral gyrus, and (D) right frontal cortex.

was observed between groups with Fazekas = 0 and Fazekas = 2 groups. Further, the subsequent analysis evaluating the correlation between severity of the WMH and atrophy rate using age as a nuisance variable showed significant positive correlations between the atrophy rate of regional gray matter and severity of WMH in the bilateral parietal and occipital cortices nearly axisymmetrically (Figure 3).

The second analysis using the data from 13 participants with hyperintensities in B&T showed only a slightly positive correlation between severity of WMHs and the atrophy rate of regional gray matter in the left parietal gyrus at the trend level (Figure 4; a seed level of $p < 0.01$ (uncorrected)).

In sum, the first analysis showed fairly axisymmetrical pattern, while the findings gained from the second analysis appear to lack systematic orderliness.

Discussion

The first analysis showed significantly positive correlations between the atrophy rate of gray matter and the severity of WMH at the baseline scan in the bilateral frontal, occipital and parietal lobes almost axisymmetrically (Figure 2). However, the second did not replicate the findings.

Previous studies showed that WMHs in any brain region cause other cortical changes (Tullberg *et al.*, 2004; Rossi *et al.*, 2006; Wen *et al.*, 2006). In addition, a study showed that there were correlations not only between WMH volume in each subdivided region and WMH volume for the overall brain, but also among each WMH volume in subdivided regions, respectively (DeCarli *et al.*, 2005). On the other hand, there are too many factors involved in the interaction to evaluate the relationship between the atrophy and the WMHs. Therefore, for the simplicity purpose, we regarded the severity of WMH for overall brain as the individual index for the subcortical WMH severity.

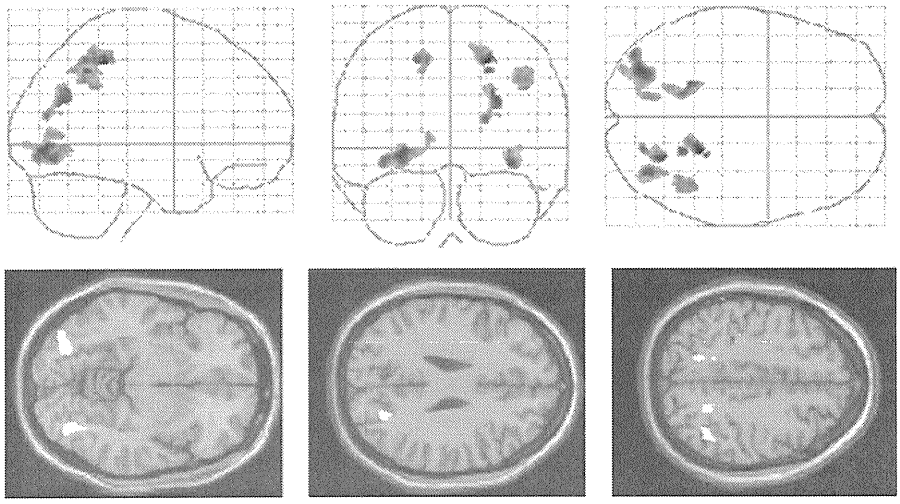

Figure 3 The relationship between the atrophy rate of regional gray matter volume and WMH severity at the baseline scan using the age as nuisance variable was evaluated in 74 participants without the hyperintensity in basal ganglia (SPM2). There were positive correlations between WMH severity and the atrophy rate of the regional gray matter volume of the bilateral occipital and parietal corti.

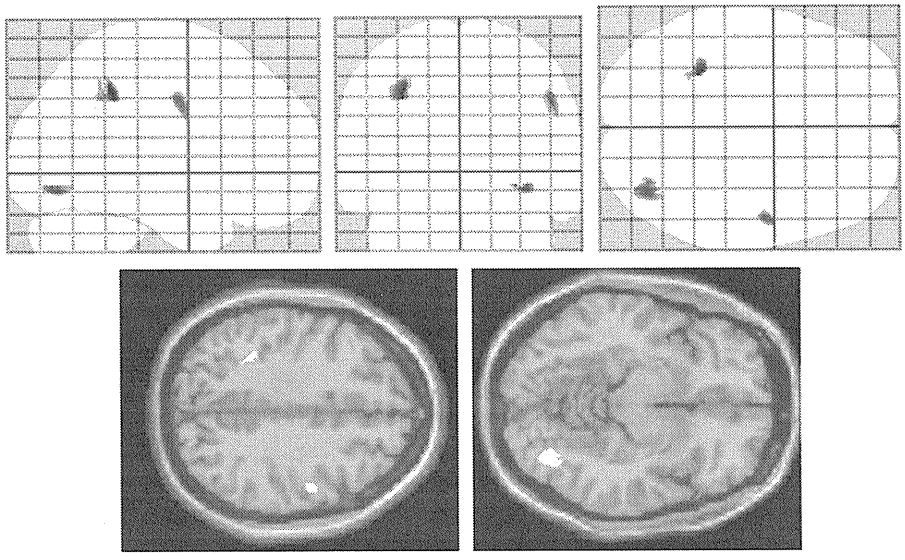

Figure 4 There was a positive correlation between severity of hyperintensity and the atrophy rate of regional gray matter volume of the left parietal cortex at the trend level in 13 participants with the severe hyperintensity in basal ganglia and thalamus.

Our results showing the relationship between the severity of WMH and the atrophy rate is compatible with previous result in general. It is known that WMH loads are likely to be observed in the white matter around the frontal horn of the lateral cerebral ventricle in the frontal lobes, and the posterior horn of the lateral cerebral ventricle in the parieto-occipital lobes, and WMH were distributed symmetrically (Wahlund *et al.*, 2001; Yoshita *et al.*, 2006). Others showed that frontal and parieto-occipital regions are the most common sites for WMH (Tullberg *et al.*, 2004; Rossi *et al.*, 2006). Our study duplicated such distribution pattern of WMH. Our result of the cerebral shrinkage and the severity of whole brain WMH might be mainly explained by the correlation between the shrinkage of the cortex in the frontal, parietal, and occipital lobes and the severity of WMH in their respective lobes. Further, the additional analysis evaluating the relationship between the severity of the WMH and atrophy rate without the aging effect showed significant positive correlations between the atrophy rate of gray matter and the severity of WMH in the bilateral occipital and parietal lobes axisymmetrically, but not in frontal regions. These fingins showed in occipito-parietal regions were nearly the same as the results not excluding the aging effect. Aging disproportionately affects frontal lobe structure, and leaving posterior and inferior brain regions relatively intact (Pfefferbaum *et al.*, 2005). In this regard, the confounding factor, aging effect, may affect these viewpoints.

Hyperintensities in the B&T mediating vast communication over widespread areas of the cortex (Mungas *et al.*, 2005; Leh *et al.*, 2007) might induce volume change in not only the brain structures *per se*, but also the connected cerebral cortices. However, previous studies paid little attention to the hyperintensities in B&T, and these results not always indicate axisymmetrical correlation. In this point, our study is the first one that investigated the WMH and cortical volume with attention to the presence or absence of the hyperintensities in B&T. When considering B&T mediate vast communication over widespread cortex (Behrens *et al.*, 2003; Mungas *et al.*, 2005), hyperintensities in B&T might induce volume change in not only the brain structures *per se*, but also the connected cerebral cortices. The second analysis using the data from 13 subjects with hyperintensities in B&T showed the asymmetrical relationship between the atrophy rate and the WMH severity. Thus, the differences in the results may be attributable to the influence of the hyperintensities in B&T.

There is a limitation in this study. First, T2 images were acquired with slice thickness of 5 mm and gap of 1.5 mm. Although our participants showed no large ischemic lesion in B&T, it might be possible that WMH from small brain structures such as thalamus and basal ganglia may not be observed. Further work using thin slice thickness and gapless T2 image will be necessary to confirm our results. Second, we did not have a large enough number of subjects with WMH loads in the basal ganglia and thalami. The procedure to extract cognitively healthy subjects through several tests might have excluded or limited the subjects with WMH lesions, which affect cognitive ability. Further studies using a large group of subjects need to be conducted. Third, previous study showed the different efficacy